รายงานวิจัยฉบับสมบูรณ์

โครงการ การวิเคราะห์โครงสร้างสามมิติและการทำแบบจำลองเชิงตัวเลข เพื่อวิเคราะห์สมบัติทางการไหลภายในโฟมโลหะไทเทเนียมแบบรูเปิด

โดย

ผู้ช่วยศาสตรจารย์ ดร. เชษฐา พันธ์เครือบุตร และคณะ

31 สิงหาคม พ.ศ. 2563

สัญญาเลขที่ TRG5880232

รายงานวิจัยฉบับสมบูรณ์

โครงการ

การวิเคราะห์โครงสร้างสามมิติและการทำแบบจำลองเชิงตัวเลขเพื่อวิเคราะห์สมบัติทางการไหลภายในโฟมโลหะไทเทเนียมแบบรูเปิด

คณะผู้วิจัย สังกัด

ผู้ช่วยศาสตราจารย์ ดร. เชษฐา พันธ์เครือบุตร
ภาควิชาวิศวกรรมโลหการ จุฬาลงกรณ์มหาวิทยาลัย

ดร. อัญชลี มโนนุกุล
ศูนย์เทคโนโลยีโลหะและวัสดุแห่งชาติ

สนับสนุนโดยสำนักงานคณะกรรมการการอุดมศึกษา และ
สำนักงานกองทุนสนับสนุนการวิจัย

(ความเห็นในรายงานนี้เป็นของผู้วิจัย สกอ. และ สกว. ไม่จำเป็นต้องเห็นด้วยเสมอไป

Executive Summary

โครงการวิจัย การวิเคราะห์โครงสร้างสามมิติและการทำแบบจำลองเชิงตัวเลขเพื่อวิเคราะห์สมบัติทางการไหลภายในโฟมโลหะไทเทเนียมแบบรูเปิด มีจุดประสงค์เพื่อศึกษาโครงสร้างสามมิติของโฟมโลหะไทเทเนียมแบบรูเปิดที่มีความพรุน (porosity) แตกต่างกันด้วยการถ่ายภาพเอกซ์เรย์สามมิติ โดยได้ทำการวิเคราะห์โครงสร้างโฟมโลหะไทเทเนียมแบบรูเปิดและคำนวณหาขนาด รูปร่าง และสัณฐานของโครงสร้าง เพื่อให้เข้าใจถึงลักษณะที่เป็นเอกลักษณ์ของโฟมโลหะไทเทเนียมแบบรูเปิดที่ผลิตจากกรรมวิธี Replica Impregnation นอกจากนั้นเพื่อศึกษาถึงผลของขนาดและรูปร่างของโครงสร้างโฟมโลหะที่มีต่อพฤติกรรมการไหลและความสามารถในการซึมผ่านได้ อันเป็นสมบัติที่สำคัญในการใช้งาน งานวิจัยนี้จึงได้ทำการสร้างแบบจำลองทางคอมพิวเตอร์จากภาพถ่ายโครงสร้างสามมิติที่ได้ เพื่อจำลองการไหลของของไหลผ่านโฟมโลหะไทเทเนียมแบบรูเปิดอีกด้วย ผลการศึกษาทั้งในส่วนของโครงสร้าง 3 มิติและพฤติกรรมการไหล ถูกยืนยันด้วยผลการวัดด้วยเทคนิคขั้นสูงและการทดลอง รวมทั้งได้ทำการเปรียบเทียบผลการศึกษาในด้านต่างๆกับงานวิจัยอื่นๆที่เกี่ยงข้องอีกด้วย

ผลการวิเคราะห์พบว่า โฟมโลหะไทเทเนียมแบบรูเปิดที่ผลิตจากกรรมวิธี replica impregnation จะมีลักษณะเฉพาะคือก้านโลหะของโครงสร้างโฟมจะมีช่องว่างภายใน ซึ่งเป็นผลมาจากต้นแบบโฟมโพลียูรีเทนรวมทั้งฟองอากาศที่เกิดขึ้นระหว่างกระบวนการผลิต ผลการค้นพบจากงานวิจัยนี้ช่วยให้สามารถเข้าใจและปรับกระบวนการผลิตโฟมโลหะให้มีคุณภาพที่สูงขึ้นได้ ผลการศึกษายังพบว่าชิ้นงานที่มีขนาดโครงสร้าง ppi ที่สูงขึ้น จะมีระดับความพรุนและขนาดของรูพรุนที่ลดลง แต่จำนวนรูพรุนจะมีเพิ่มขึ้น นอกจากนั้นผลการวัดค่า aspect ratio และ orientation ของรูพรุนทำให้สามารถยืนยันได้ว่า โครงสร้างโฟมโลหะไทเทเนียมแบบรูเปิดที่ผลิตจากกรรมวิธี replica impregnation มีลักษณะที่ไม่สมมาตร (geometry anisotropy) ในสามมิติอีกด้วย ซึ่งลักษณะที่ไม่สมมาตรนี้มีผลอย่างมากต่อการใช้งานบางประเภท

งานวิจัยนี้ยังได้ใช้แบบจำลองทางคอมพิวเตอร์เพื่อจำลองการไหลภายในโครงสร้างโฟมโลหะ และหาความสัมพันธ์ระหว่างลักษณะโครงสร้างกับพฤติกรรมของการไหล ซึ่งผลการศึกษาจากแบบจำลองพบว่าความสามารถในการซึมผ่าน (permeability) ในทิศทางการไหลที่ขนานกับทิศทางการขึ้นรูปของชิ้นงาน (foaming direction) มีค่าสูงกว่า เมื่อเทียบกับการไหลที่ตั้งฉากกับทิศทางการขึ้นรูปของชิ้นงาน ทำให้ยืนยันได้ว่า ลักษณะที่ไม่สมมาตรของโครงสร้างโฟมโลหะไทเทเนียม ส่งผลโดยตรงต่อพฤติกรรมของการไหลที่ไม่เท่ากันในแต่ละด้าน ผลที่ได้จากงานวิจัยนี้เป็นข้อมูลที่สำคัญในการออกแบบโครงสร้างโฟมโลหะไทเทเนียมที่เหมาะสมต่อการใช้งานทางวิศวกรรมที่มีฟังก์ชันการใช้งานที่ซับซ้อนและการแพทย์ต่อไป

บทคัดย่อ

โฟมโลหะไทเทเนียมแบบรูเปิดเริ่มได้รับความสนใจมากขึ้นจากภาคอุตสาหกรรมในการนำมาใช้งานทางด้านชีวการแพทย์และชิ้นส่วนวิศวกรรมที่มีฟังก์ชันที่ซับซ้อน เนื่องจากมีความเบาจากโครงสร้างแบบรูพรุน รวมทั้งมีสมบัติทางด้านกายภาพและทางกลที่ดี ในงานวิจัยนี้ได้นำเทคนิคการถ่ายภาพเอ็กซ์เรย์แบบสามมิติมาใช้ในการวิเคราะห์โครงสร้างสามมิติของชิ้นงานโฟมโลหะไทเทเนียมแบบรูเปิดที่ผลิตจากกรรมวิธี replica impregnation ชิ้นงานโฟมโลหะไทเทเนียมแบบรูเปิดที่มีระดับความพรุนที่แตกต่างกัน 4 ระดับ ถูกผลิตจากต้นแบบโฟมโพลียูรีเทนที่มีขนาดโครงสร้าง 25-40 ppi โดยข้อมูลจากเทคนิคการถ่ายภาพเอ็กซ์เรย์แบบสามมิติของทั้ง 4 ชิ้นงาน ถูกนำมาวิเคราะห์เพื่อศึกษาถึงลักษณะและรูปร่างของรูพรุนภายในโครงสร้างโฟมโลหะรวมทั้งก้านโลหะไทเทเนียม ผลการวิเคราะห์พบว่า โฟมโลหะไทเทเนียมแบบรูเปิดที่ผลิตจากกรรมวิธี replica impregnation จะมีลักษณะเฉพาะคือก้านโลหะของโครงสร้างโฟมจะมีช่องว่างภายใน ซึ่งเป็นผลมาจากต้นแบบโฟมโพลียูรีเทนรวมทั้งฟองอากาศที่เกิดขึ้นระหว่างกระบวนการผลิต ผลการศึกษายังพบว่าชิ้นงานที่มีขนาดโครงสร้าง ppi ที่สูงขึ้น จะมีระดับความพรุนและขนาดของรูพรุนที่ลดลง แต่จำนวนรูพรุนจะมีเพิ่มขึ้น นอกจากนั้นผลการวัดค่า aspect ratio และ orientation ของรูพรุนทำให้สามารถยืนยันได้ว่า โครงสร้างโฟมโลหะไทเทเนียมแบบรูเปิดที่ผลิตจากกรรมวิธี replica impregnation มีลักษณะที่ไม่สมมาตร (geometry anisotropy) การศึกษาด้วยภาพถ่ายจุลทรรศน์แบบใช้แสงและแบบอิเล็กตรอนยืนยันลักษณะความไม่สมมาตรของชิ้นงาน ในงานวิจัยนี้ยังได้ทำการสร้างแบบจำลองทางคอมพิวเตอร์เพื่อจำลองการไหลภายในโครงสร้างโฟมโลหะ และหาความสัมพันธ์ระหว่างลักษณะโครงสร้างกับพฤติกรรมของการไหล ผลการศึกษาพบว่าความสามารถในการซึมผ่าน (permeability) ในทิศทางการไหลที่ขนานกับทิศทางการขึ้นรูปของชิ้นงาน (foaming direction) มีค่าสูงกว่า เมื่อเทียบกับการไหลที่ตั้งฉากกับทิศทางการขึ้นรูปของชิ้นงาน ทำให้ยืนยันได้ว่าลักษณะที่ไม่สมมาตรของโครงสร้างโฟมโลหะไทเทเนียม ส่งผลต่อพฤติกรรมของการไหลที่ไม่เท่ากันในแต่ละด้าน ผลที่ได้จากงานวิจัยนี้เป็นข้อมูลที่สำคัญในการออกแบบโครงสร้างโฟมโลหะไทเทเนียมที่เหมาะสมต่อการใช้งานทางวิศวกรรมที่มีฟังก์ชันการใช้งานที่ซับซ้อนและการแพทย์ต่อไป

คำสืบค้น : โฟมโลหะไทเทเนียม เทคนิคการถ่ายภาพเอ็กซ์เรย์แบบสามมิติ แบบจำลองการไหล ความสามารถในการซึมผ่าน

Abstract

Open-cell titanium foams have been receiving growing attention from the industrial to be used in biological and functional engineering applications due to their lightweight porous structure with excellent physical and mechanical properties. In this research, the x-ray tomography technique was used to characterise actual structure of open-cell titanium foams, manufactured from replica impregnation method, in three-dimensional (3D). Titanium foams with four different porosity, produced using polymer template with porosity of 25-40 ppi (pore per linear inch), were analysed to quantify structural parameters and morphological geometries of open-cell pores and titanium struts. It was found that titanium foam manufactured from replica impregnation method has the characteristic hollow strut, containing polyurethane voids and air bubbles. As the template cell size (ppi) increased, porosity and average pore diameter decreased whereas the number of individual pores increased. The measured aspect ratio and orientation of pores indicated geometry anisotropy of titanium foams. Microstructure evaluation using scanning electron microscope and 3D optical microscope confirmed geometry anisotropy of the structure. The numerical analysis and permeability assessment of fluid flow were also performed to investigate the relationship between structural parameters and flow behaviour. The permeability was significantly higher for the flow parallel to foaming direction as compared to the flow perpendicular to foaming direction, confirming that degree of geometry anisotropy was sufficient to cause significant flow property anisotropy. This better insight is of great importance to design the optimal structure for various functional applications.

Keywords: Titanium foams, X-ray tomography, Flow simulation, Permeability

Table of Contents

Topic

Page

Chapter 1 Introduction and literature review....1

1.1 Introduction to research problem and its significant....1

1.2 Objectives....2

1.3 Scope of research....2

1.4. Literature reviews....3

1.5 Expected benefits....6

Chapter 2 Methodology....7

2.1 Specimen preparation....7

2.2 X-ray tomography....7

2.3 Characterisation of three-dimensional titanium foam structures....8

2.4 Numerical simulation of fluid flow through open-cell titanium foams....9

Chapter 3 Results and Discussions....12

3.1 Characterisation of three-dimensional titanium foam structures....12

3.1.1 Characteristic of titanium foam produced by replica impregnation method 12

3.1.2 Porosity of titanium foams with different cell sizes....16

3.2 Pore analysis and geometry anisotropy....19

3.2.1 Pore size and number of pores....19

3.2.2 Geometry anisotropy....22

3.3 Pore distribution and strut network....24

3.4 Fluid flow simulation....28

3.4.1 Flow velocity through open-cell titanium foams....29

3.4.2 Permeability assessment of titanium foams....31

Conclusion....33

References....35

Chapter 1

Introduction and literature review

1.1 Introduction to research problem and its significant

Recent advance development in metal foam processing has enabled the usage of the lightweight cellular metals in many engineering applications. In biomedical industry, metal foams of titanium and its alloys are highly considered to be used for human bone replacement due to their excellent strength-to-weight ratio, corrosion resistance and biological properties. The advantage of lightweight porous structure with interesting combination of physical and mechanical properties also makes titanium foam a potential candidate for new functional engineering applications, ranging from electrolysis systems, filtration and compact heat exchanger in electronics and automotive industries.

These functional engineering applications are generally used under load-bearing conditions and/or subjected to thermal/fluid transport. Despite recognising that porous structure (pore and strut sizes) and morphological geometries are crucial to mechanical performance and could be critical in influencing fluid flow, only limited studies have been done on three-dimensional (3D) structural characterisation. There are even less work on the numerical analysis of the transport in these non-ideal 3D structures.

To design the optimal structure for various functional applications, quantifying key structural parameters, such as pore/strut sizes and connectivity, of titanium metal foams is essential. It is also important to correlate them to the flow transport. Therefore, the characterisation of actual 3D structures together with the understanding of relationship between structural parameters and flow behaviour (e.g. permeability) is of great importance.

1.2 Objectives

(1) Perform x-ray tomographic experiments to acquire three-dimensional open-cell structures of titanium foams with different porosity levels.

(2) Characterise the open-cell structure parameters (such as pore and strut sizes) and morphological geometries (such as porosity and connectivity) using novel 3D image analysis technique.

(3) Develop tomographic-based model for the numerical simulation of fluid flow through open-cell titanium foams.

(4) Study the influence of structure parameters on flow behaviour and permeability.

1.3 Scope of research

(1) This project will focus the study on the 3D structural characterisation of open-cell titanium foams manufactured from replica impregnation method. Four specimens having different porosity levels, using polymer template with porosity of 25-40 ppi, will be scanned and analysed using x-ray tomography technique. The titanium foam specimens will be pre-manufactured from MTEC laboratory and hence processing parameters of replica impregnation foaming method will not be considered in this work.

(2) In this research project, the tomographic-based CFD simulation of flow through open-cell structures will be performed on all four specimens with the same size of representative elementary volume (REV). The simulation domains will be in three-dimensional and the flow studies will be carried out in each of the three directions along the x, y and z axes. The Navier–Stokes equation in this CFD will be simplified by assuming steady-state flow, incompressible flow and linear relationship between viscous drag and fluid velocity. Permeability will be calculated based on Darcy's Law.

(3) The simulated flow results will be used to correlate the influence of structure parameters on flow behaviour and permeability.

1.4. Literature reviews

Titanium and its alloys have been used extensively in many engineering applications including aerospace components and biomedical implants due to their excellent strength-to-weight ratio, high corrosion and oxidation resistance, and favourable biocompatibility [1, 2]. Recently, several methods for manufacturing metal foams and other porous metallic structures have become more available [3-7]. In particular, powder metallurgy (PM) route has been widely used as a common method to produce titanium foams for many engineering usage [8]. Of many PM methods, additive manufacturing with metal powders [9, 10], powder sintering with foaming agent [11, 12], powder sintering with space holder [13-15], and replica impregnation [16, 17] methods present great ability to shape complex titanium porous structures with varied levels of porosity. Although all four methods can produce open-cell titanium foams, previous studies [9, 10, 17] have shown that it is difficult to achieve highly porous structure with uniform connected pore network using foaming agent or space holder foaming methods. It is, however, possible to produce uniform open-cell titanium foam with high level of porosity using additive manufacturing (e.g. selective laser melting) and replica impregnation methods, as shown in Figure 1.

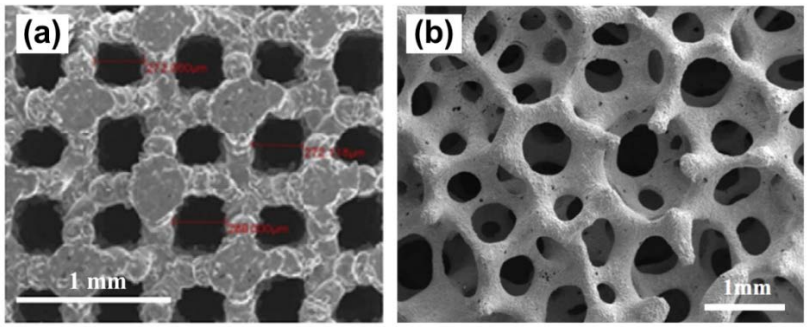

Figure 1 SEM micrographs showing open-cell structure of titanium foams manufactured from (a) selective laser melting [10] and (b) replica impregnation methods [17].

As the additive manufacturing approach uses computer aided design to directly produce titanium foam by selectively melting powder bed layer by layer, almost-ideal

connected pore network and complex features of the titanium foam structure can be achieved. However, this technology is rather slow and expensive. Therefore, its usage is only limited to medical orthopedic applications and prototyping components. Alternatively, replica impregnation method offers a processing route that is more cost-effective and amenable to mass production. Prior study [17] also showed promising results that titanium foams with good compressibility and high strength can be manufactured by replica impregnation method. The porous network of titanium foam produced via this method is, however, non-ideal.

Open-cell metal foams are mainly used in functional applications where the nature of continuous porous network is of great benefit to thermal/fluid transport conditions. For example, in biomedical industry, titanium foam (scaffold) with high porosity structure is preferred to aid nutrient delivery for bone ingrowth [18, 19]. In other engineering industries, open-cell metal foams are used for applications ranging from acoustic absorption components, heat exchangers, gas/fluid filters and electrodes in electrolysis system [3, 4, 20-24]. The difference in final porous structure, resulting from different processing parameters, can greatly affect both mechanical [6, 15] and flow properties, which are important to the performance of the functional applications. Experimentally, it has been shown that structural parameters (e.g. cell size and porosity) have significant effects on heat transfer properties [21, 25, 26] and flow behaviour (e.g. permeability) [27-30]. Therefore, there is a strong need to quantify morphological geometries of the actual metal foams.

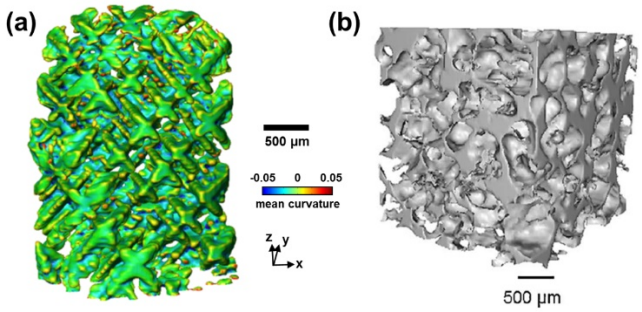

Figure 2 Three dimensional rendering of (a) solidifying dendritic structure of Al-Si alloy [31] and (b) porous structure of titanium foam produced by space holder method [15].

X-ray computed tomography (μ-CT or XMT) is an effective characterisation technique that is capable of imaging, nondestructively, three-dimensional interior structure of materials [31-33], as shown in Figure 2(a). This method has been recently used to investigate cellular materials (as illustrated in Figure 2(b)), enabling accurate quantification of pore and strut networks as well as pore connectivity of metal foams [10, 15, 34]. Previous morphological analysis of aluminium foams using XMT also highlighted that actual structure of metal foams is highly-irregular and also revealed that some assumptions taken from ideal geometry model is inaccurate [35]. This suggests that numerical simulations performed on periodic unit-cell structures (such as [36, 37]) may not be adequate to capture the intricate details of flow and transport in the actual irregular porous structures.

To accurately study the relationship between structural parameters and flow/transport behaviour, the real structures acquired from x-ray tomography were employed as starting domains for computational fluid dynamics (CFD) analysis [26, 29, 31, 38]. This combination of XMT and numerical simulation (also referred to as tomography-based simulation or image-based simulation) has been recently used to investigate fluid flow and heat transport through open-cell aluminium and copper foams [29, 39-41]. Figure 3 demonstrates some examples of tomography-based simulation in aluminium foams. Although there has also been few studies on fluid transport through open-cell titanium foams [18, 19], those studies mainly focused on conditions tailored for biomedical applications.

In order to extend our understanding of the relationship between structure parameters and flow behaviour in other functional engineering applications, such as those in electrolysis system, further study on 3D structural characterisation and image-based simulation in broader flow conditions is required.

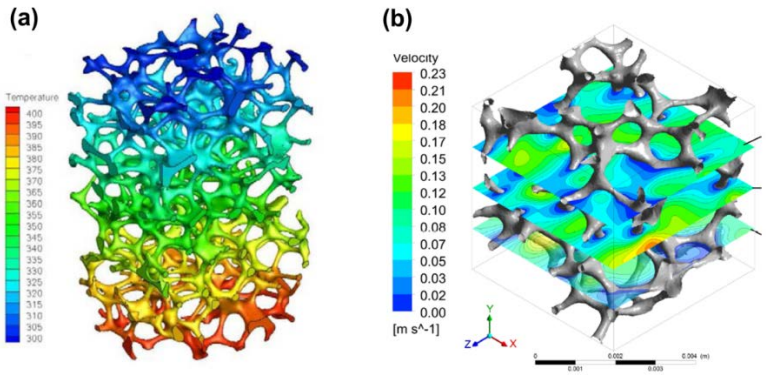

Figure 3 Tomography-based simulations performed on aluminum foams for (a) heat transport [39] and (b) fluid flow analysis [41]

1.5 Expected benefits

(1) The 3D characterization of open-cell titanium foams allows their structure parameters (e.g. pore and strut sizes) and morphological geometries (e.g. porosity and connectivity) to be accurately quantified. This 3D characterisation technique not only provide improved insights into porous structure of titanium but could also offer a new way to investigate the quality of manufactured titanium foams.

(2) The influence of structure parameters on flow behaviour and permeability was studied in this project. This understanding is of great importance to the development of titanium metal foams for new functional engineering applications with better performance.

(3) The developing method of tomography-based fluid flow simulation for open-cell titanium foams could be further extended to calculate fluid/heat transport in other porous metals, such as aluminium and copper foams. This is critical to design metal foams for a broader range of functional engineering applications in the future.

Chapter 2

Methodology

2.1 Specimen preparation

Four specimens of open-cell titanium foams produced from replica impregnation method using polymer template with porosity of 25-40 ppi was first prepared (titanium foam samples produced by this technique is shown in Figure 4) and wire cut into cylindrical shape (8 cm diameter and 8 cm height) for subsequent imaging. As detailed in [17], replica impregnation method uses titanium slurry (mixture of titanium powder, water, and binder) to impregnate open-cell polymer foam template. After removing excess slurry by squeezing, the green titanium foams were dried in air, then debound in argon atmosphere, and finally sintered under high vacuum.

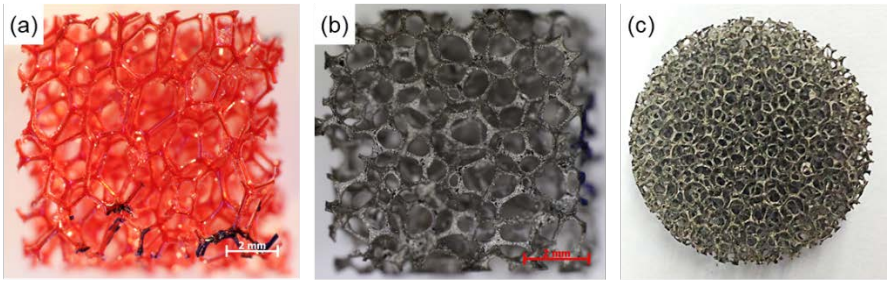

Figure 4 Open-cell titanium foams produced from replica impregnation method: (a) polyurethane template (b) sintered titanium foam (c) cylindrical titanium foam specimen

2.2 X-ray tomography

The prepared foam specimens were scanned, using commercial x-ray tomography machine, at high spatial resolution (approximate resolution of 5 μm/voxel) to ensure all details of pores and solid titanium networks to be captured. In each x-ray tomography scan, a series of two-dimensional x-ray images (radiographs) was first taken at different illumination angles

(angular range of 360°). These images were then be digitally reconstructed to obtain three-dimensional cellular structure of a foam specimen, as shown in Figure 5.

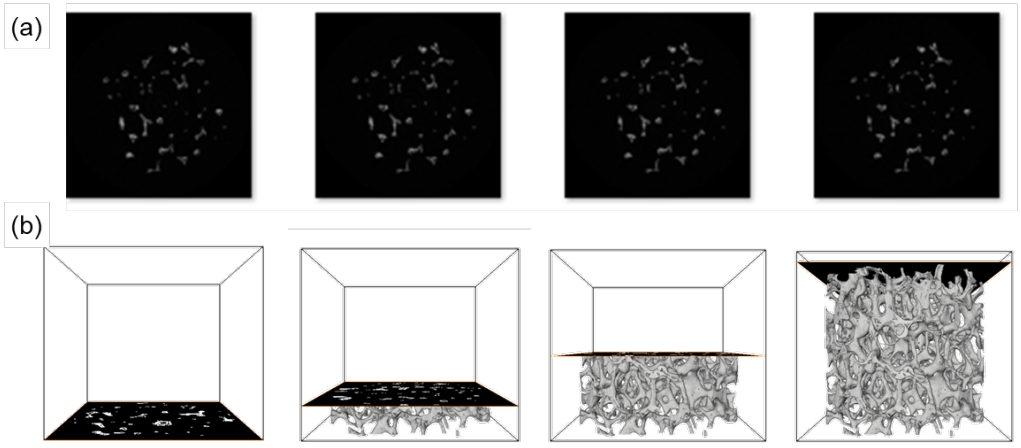

Figure 5 (a) 2D reconstructed slices obtained from x-ray tomography (b) 3D rendering of titanium porous structure from stack of 2D reconstructed slices

2.3 Characterisation of three-dimensional titanium foam structures

After tomography acquisition, each reconstructed 3D volume was first processed with edge-preserving smoothing algorithm to remove the noise in the scans and to enhance image contrast. Subsequently, the filtered 3D volumes were segmented (binarised) using region-growing thresholding method. This segmentation process was done to identify the regions of solid networks and pores. Finally, novel image processing techniques (combination of Euclidean distance transforms, watershed algorithm, skeletonization algorithm and principal component analysis) [33, 42] were used to characterise the open-cell structure parameters and morphological geometries such as pore size distribution, pore anisotropy, strut size distribution, strut connectivity and porosity. Manufacturing defects (e.g. polyurethane space and entraped bubbles inside titanium strut) were also examined. These quantification processes were performed using Matlab (MathWorks, MA) and Avizo (Thermo Fisher Scientific, MA) software. Optical microscopy and scanning electron microscopy were also performed to validate the quantification results.

2.4 Numerical simulation of fluid flow through open-cell titanium foams

The segmented 3D structure of each specimen was used as input geometries for the tomographic-based numerical simulations of fluid flow through open-cell foams. Note that the input for CFD simulation was selected as representative element volume (REV) of size 4x4x4 mm^3, as shown in Figure 6(a), from the entire cylindrical specimen to reduce computational time. This size of REV has been verified to confirm good representative volume of the entire structure. First, the finite volume mesh (tetrahedron elements) of the flow regions (pore space in 3D volume) was created, as illusted in Figure 6(b). Next, flow stabilized zone (Figure 6(c)), boundary conditions (Figure 7), and fluid properties were set in the model to match conditions found in real functional engineering applications. Finally, the commercial computational fluid dynamics (CFD) package - Ansys Fluent (Ansys Inc., PA) was used to solve flow problem based on full Navier–Stokes equation. This method will enable the flow behaviour and permeability to be determined for each 3D volume with different structure parameters.

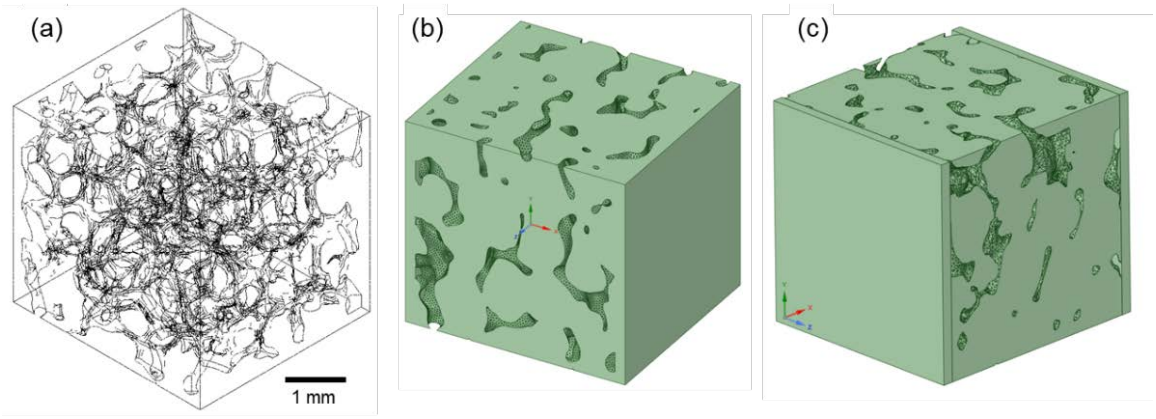

Figure 6 Numerical simulation of fluid flow (a) segmented 3D structure of open-cell titanium foam, (b) flow region, and (c) flow region with stabilized zones at inlet and outlet

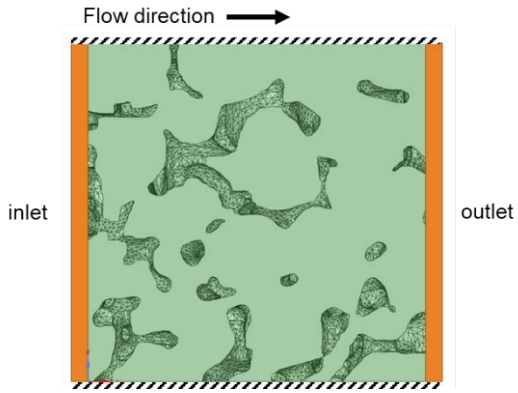

Figure 7 Boundary conditions of fluid flow simulation

Flow resistance of an incompressible Newtonian fluid through a open-cell titanium foam can be measured by the excess pressure ΔP (i.e. different in pressure at flow inlet and outlet) that must be applied to cause steady state fluid flow with a given unidirectional average velocity through a unit length of the porous medium. The law governing such unidirectional fluid flow is the Dupuit–Forchheimer modification of Darcy's law:

$$-\frac{\partial P}{\partial x} = \frac{\mu}{K} v_0 + \rho C v_0^2 \qquad \text{(Equation 1)}$$

where P is pressure in fluid, x is distance along the direction of fluid flow, μ is the fluid viscosity, v_0 is fluid velocity and ρ is fluid density. The Darcian permeability K and the form coefficient C are characteristics of the porous medium. At low fluid velocities, Equation (1) simplifies to Darcy's law:

$$v_0 = -\frac{\partial P}{\partial x}\frac{K}{\mu} \qquad \text{(Equation 2)}$$

In this research, the fluid is modelled as water. The viscosity is 0.001 Pa·s, density is 998.2 kg/m3. Boundary conditions of the flow were assumed as follow: zero pressure outlet, velocity inlet of 0.0001 m/s, and no-slip wall condition. The change in pressure across open-cell titanium foam was determined from the numerical simulation and subsequently used to calculated permeability (K) using Darcy's law (Equation 2).

To validate the calculated permeability, physical evaluation of fluid flow through open-cell titanium foams was performed using experimental setup shown in Figure 8-9.

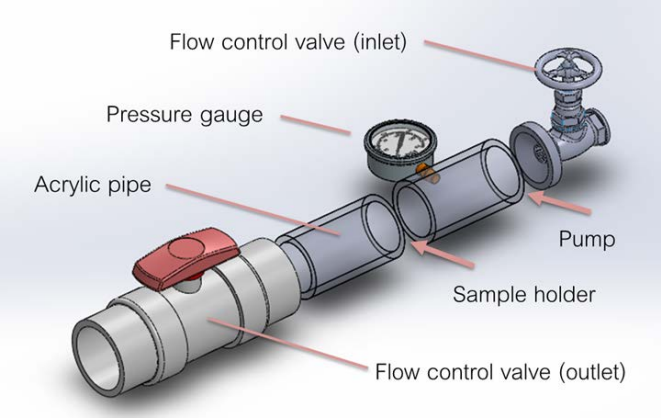

Figure 8 Schematic of the permeability measurement apparatus

The volumetric flow rate was estimated by measuring the time to fill a container of precisely known volume (1 liter of distilled water). The measurement of the flow rate was obtained from 10 experiments to ensure the consistancy. The inlet pressure was fixed at a given value and the outlet pressure was assumed atmospheric pressure. The titanium foam sample was sealed into the sample holder, as shown in Figure 9, to ensure that there was no fluid flows along the outer side-surface of the specimens

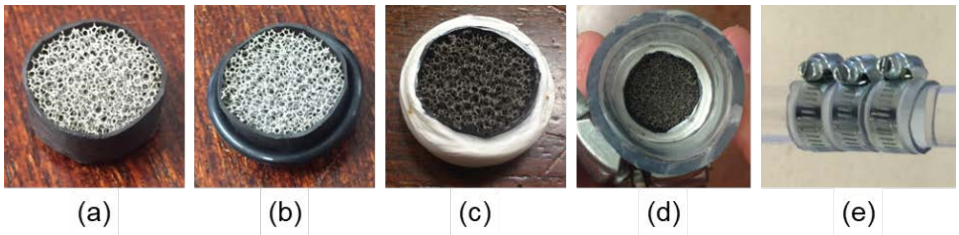

Figure 9 Sample holder for permeability measurement (a) titanium foam sealed into a heat-shrinkable polymer tube, (b) fitted with rubber O ring, (c) sealed by Teflon tape (d) mounted to rubber hose pipe (e) holder tightened by metal strap

Chapter 3

Results and Discussions

3.1 Characterisation of three-dimensional titanium foam structures

3.1.1 Characteristic of titanium foam produced by replica impregnation method

Approximately 2000 CT reconstructed images were collected for each metal foam sample. The image sizes covered the entire volume of the specimen (8 cm diameter and 8 cm height). Using histogram-based and region-growing based segmentation, there were 3 regions identified and labelled for further analysis. 3D rendering of these regions is shown in Figure 10. The first region is actual titanium structure with hollow strut, Figure 10(a), the second region is empty space inside titanium structure that used to by polyurethane template, Figure 10(b), and the third region is empty space inside titanium structure that referred to air bubbles entrapped during replica impregnation processing, Figure 10(c).

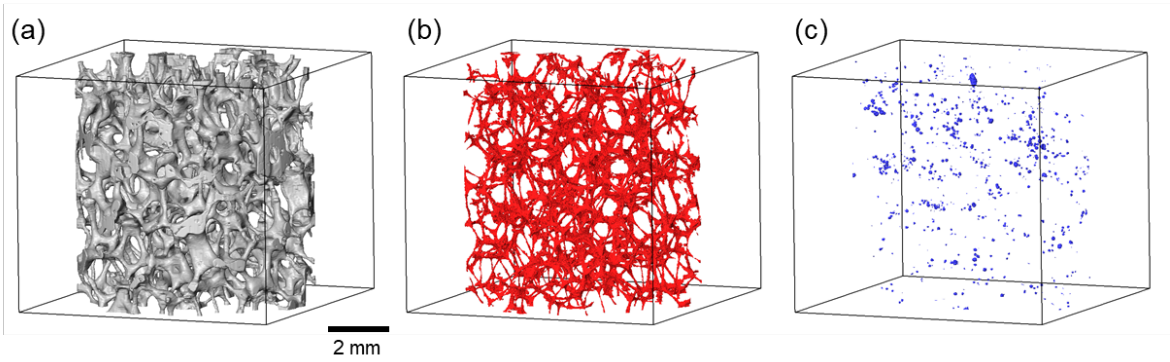

Figure 10 3D rendering of (a) titanium foam structure with 30 ppi cell size having hollow strut, (b) space inside titanium strut from polyurethane template and (c) space inside titanium strut from air bubbles

Figures 11-13 illustrates these identified regions in all four specimens having cell size ranging from 25 to 40ppi.

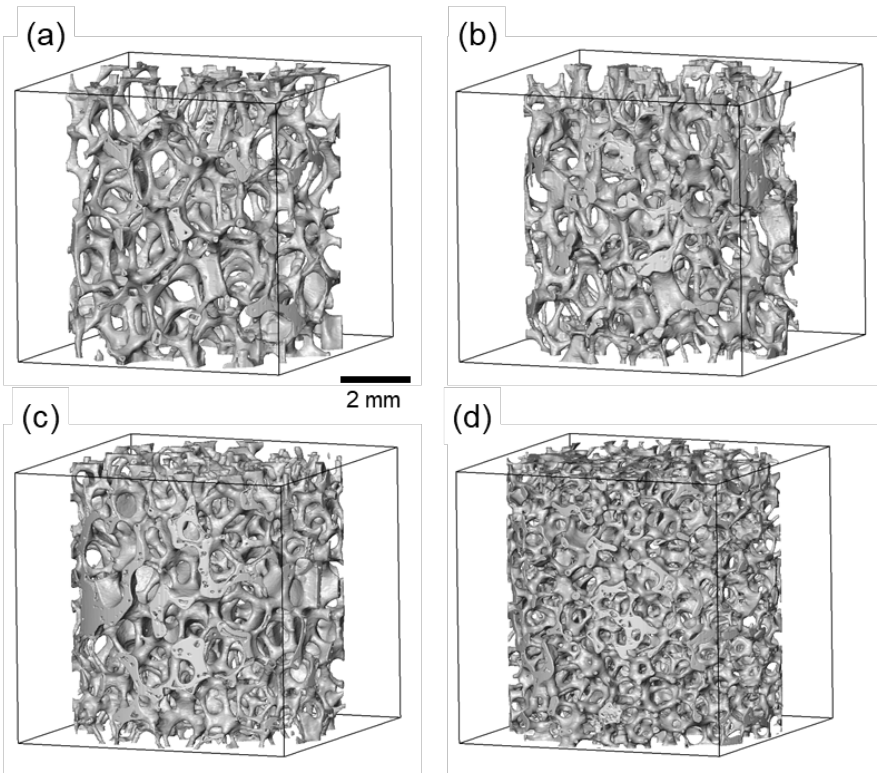

Figure 11 Titanium foam structure: (a) 25ppi (b) 30 ppi (c) 35ppi (d) 40ppi

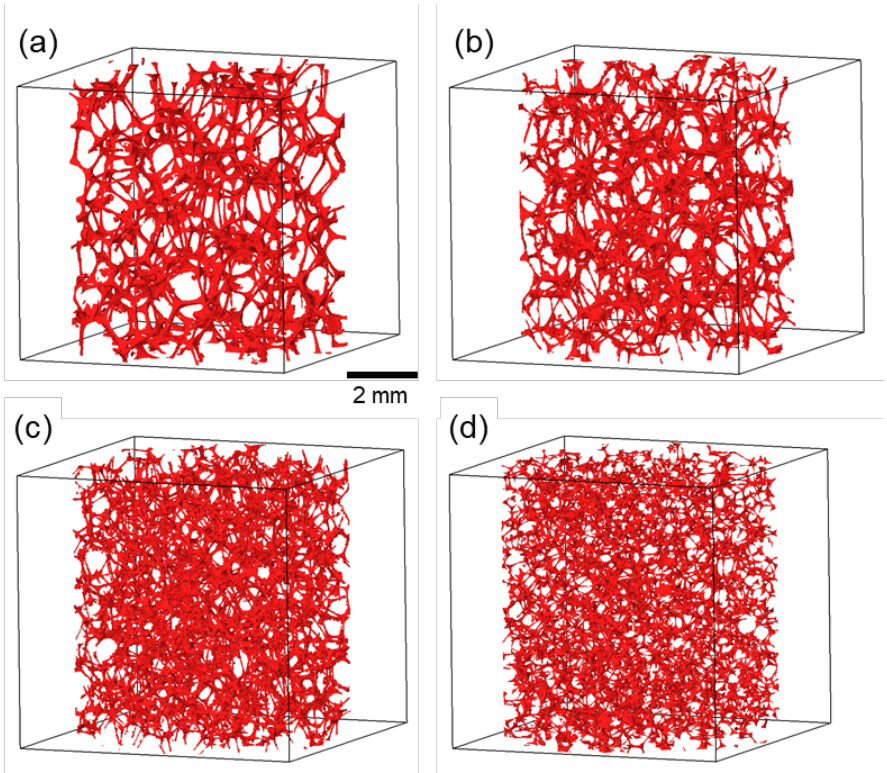

Figure 12 Polyurethane space inside titanium strut: (a) 25ppi (b) 30 ppi (c) 35ppi (d) 40ppi

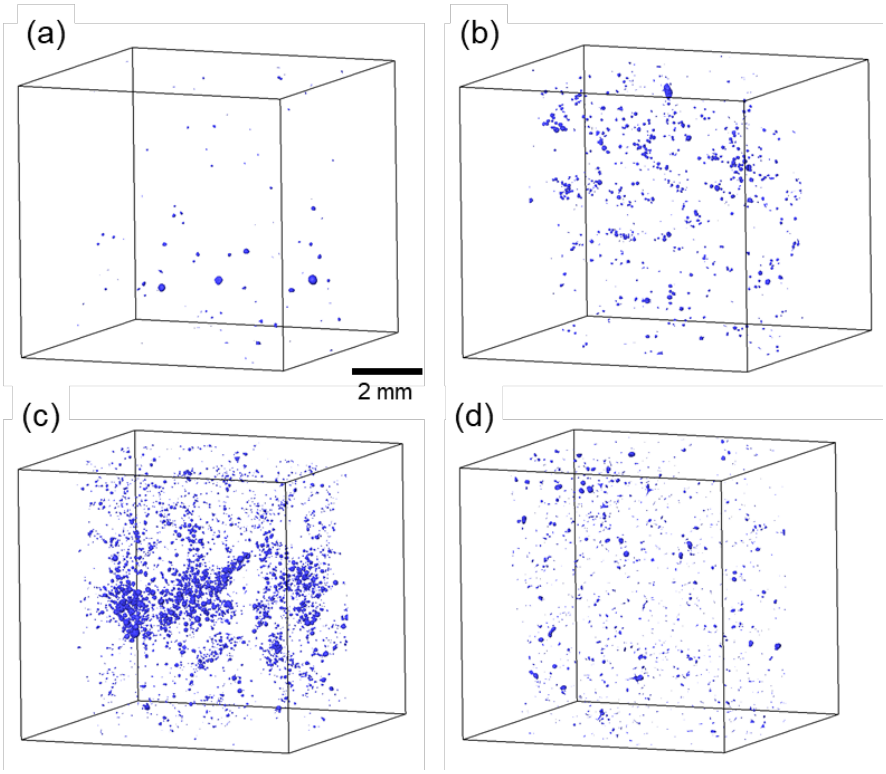

Figure 13 Air bubbles inside titanium strut: (a) 25ppi (b) 30 ppi (c) 35ppi (d) 40ppi

These results confirm that all titanium foams made from replica impregnation method have hollow struts owing to its processing technique. The characteristic polyurethane space (Figure 12) is unavoidable since the polymer was used as template for titanium slurry coating. This template was decomposed during sintering process, leaving empty space inside the titanium strut. The geometry of this polyurethane space is a replica of the titanium foam structure. The size of polyurethane space is observed to be smaller compared to original polyurethane template since significant shrinkage is expected during heating and sintering processes. It can also be seen that there are several polyurethane spaces that connected to the outer surface of titanium strut. This indicates that polyurethane template was not well covered by titanium powder in some areas, particularly near the interconnect of struts.

Air bubbles inside titanium strut can be found throughout all specimens, as shown in Figure 13. During titanium slurry coating process, it is possible that air entrapement occurs and air bubbles remain after the process. It is observed that the geometry of these

bubbles is quite round and mostly spherical. This confirms that the origin of this empty space was air bubbles since the bubbles are spherical in shape due to its high surface tension. It is also worth noting that there seems to be no correlation between the amount of air bubbles and titanium foam with increasing cell sizes. In this research, titanium foam specimen with 35ppi cell size contains the largest amount of air bubble space, representing the lowest manufacturing quality. The amount of air bubbles could be minimised by having a good process control during mixing and coating of titanium slurry.

Scanning electron microscopy (SEM) was also performed on the titanium foam sample with 30 ppi cell size to confirm the evidence of polyurethane space and air bubbles that were appeared on the outer surface of titanium struts. Figure 14 illustrates that triangular voids can be found at the interconnects and small rounded voids can be found along the struts though out the sample. This confirms that polyurethane template in some area was not well covered by titanium powder, particularly near the interconnect of struts, and air bubbles created during mixing and coating processes were tended to locate close to surface of titanium struts.

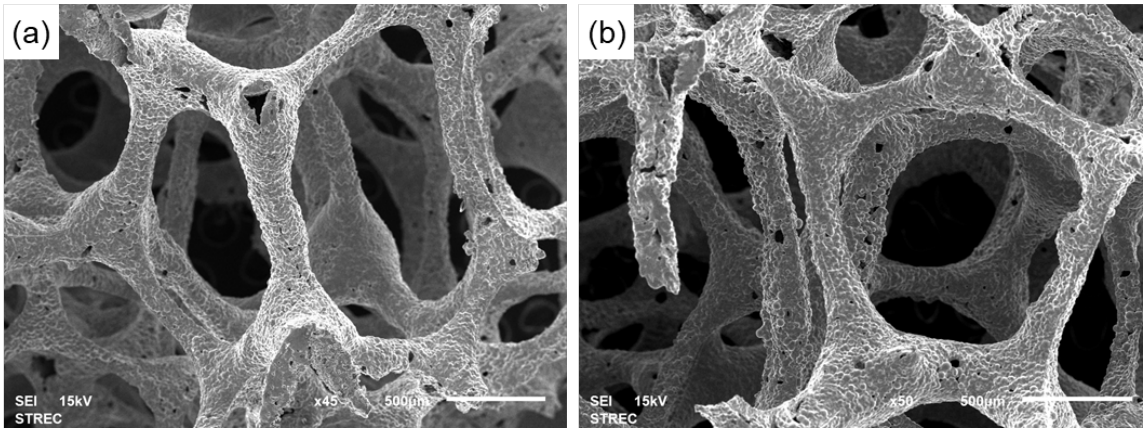

Figure 14 Surface-connected voids in titanium foam 30 ppi sample made by replica impregnation method: (a) triangular void at the interconnect (b) voids along the struts

Quantification of 3D volume of the identified regions was also performed to investigate volume perentage of titanium foam with hollow strut, polyurethane space, and air bubbles in the samples with different cell sizes, as shown in Figure 15. It can be clearly observed that volume of titanium structure increases uniformly with decreasing cell size (i.e. increasing ppi). The volume of titanium structure increases from 9.19% in 25 ppi cell size to 14.81% in 40 ppi cell size. The volumes of polyurethane space and air bubbles are in a range of 1.2-1.6% and 0.01-0.2%, respectively.

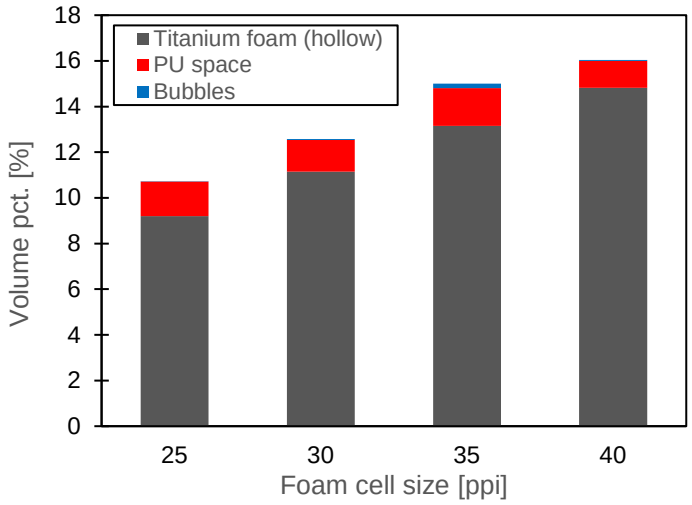

Figure 15 Volume percentage of titanium foam with hollow strut, polyurethane space, and air bubbles in the samples with different cell sizes

3.1.2 Porosity of titanium foams with different cell sizes

As seen from previous section, titanium foam manufactured from replica impregnation method has the characteristic hollow strut. This characteristic does not exist in titanium foams from other manufacturing techniques; thus, the measured porosity level of titanium impregnaiton foams might not be in a direct comparison to other titanium foams. Therefore, two methods were applied in this work to investigate porosity level of titanium foams with different cell sizes. First, the measurement was performed on the actual titanium foam structure having hollow strut (i.e. Figure 11). Second, the measurement was performed

on the modified titanium foam structure having solid strut (i.e. filled hollow space). In order to obtain the modified titanium foam structure, all three regions of titanium foam with hollow strut, polyurethane space, and air bubbles are combined, as shown in Figure 16.

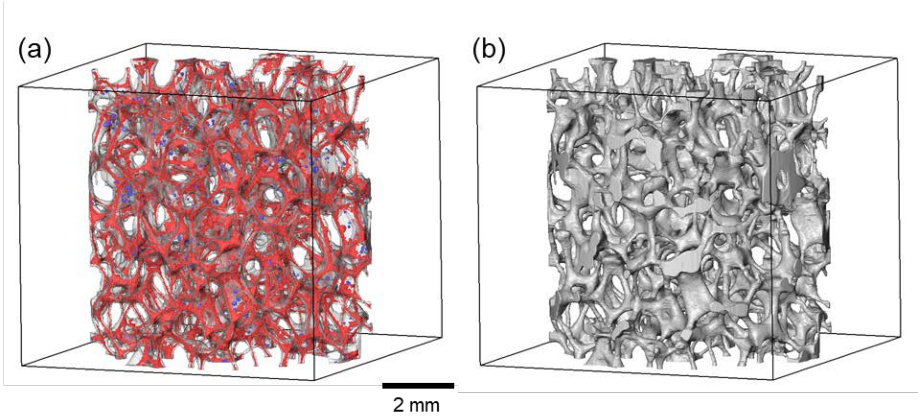

Figure 16 (a) Actual titanium foam containing polyurethane space (highlighted red) and air bubbles (highlighted blue) inside its hollow strut, and (b) modified titanium foam having solid strut (filled hollow space)

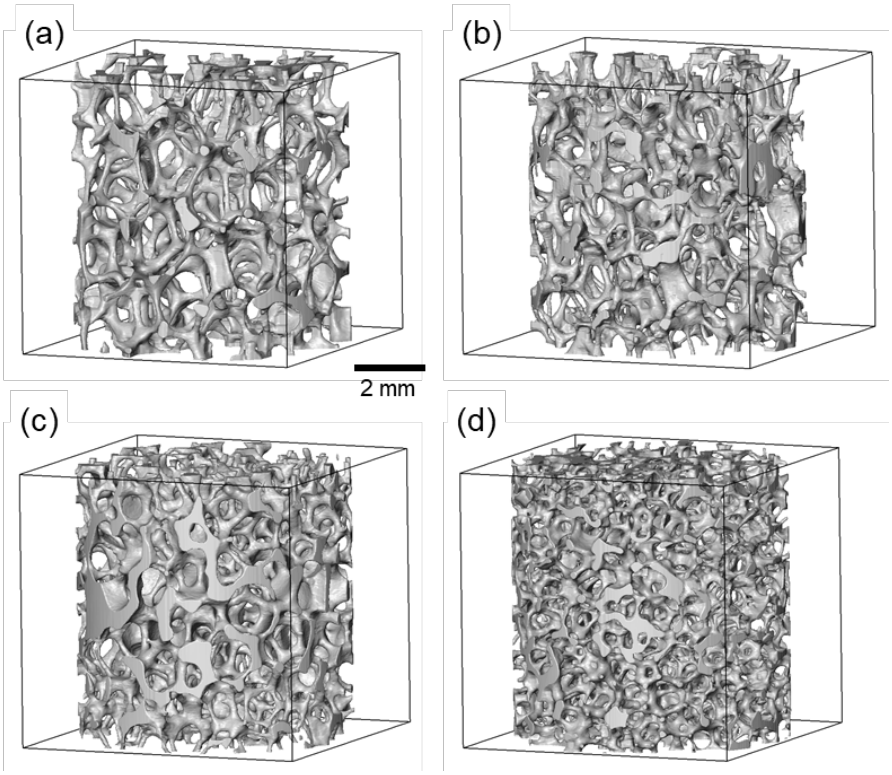

Figure 17 Titanium foam structure with filled strut: (a) 25ppi (b) 30 ppi (c) 35ppi (d) 40ppi

Figure 17 illustrates 3D rendering of the modified titanium foam structures with filled strut in all four specimens. It can be clearly observed that volume of titanium structure increases uniformly with decreasing cell size (i.e. increasing ppi). This is expected since there were more struts per volume in higher ppi polyurethane foam for titanium slurry to impregnate. This agrees well with previous work reported that apparent density of titanium foams made by the same method increases with increasing ppi [43].

The measurements of porosity level in all specimens, both hollow and filled strut structure, are shown in Figure 18. As the number of pores (ppi) increased, the porosity decreased uniformly, both in filled and hollow titanium foams. Similar results (Manonukul et al. [43, 44]) have also been reported that level of porosity decreases with higher ppi. Although, those works used density measurement method to estimate for porosity, the measured values agree well with the 3D measurement in this work. Note that hollowed titanium foams can only be compared to previous density measurement method as it represents the acutal titanium foam structure without having image processing methods for strut filling. As expected, the porosity in filled titanium foams is lower compared to that of hollowed titanium foams. This corresponds to the filled volume of polyurethane void and bubbles.

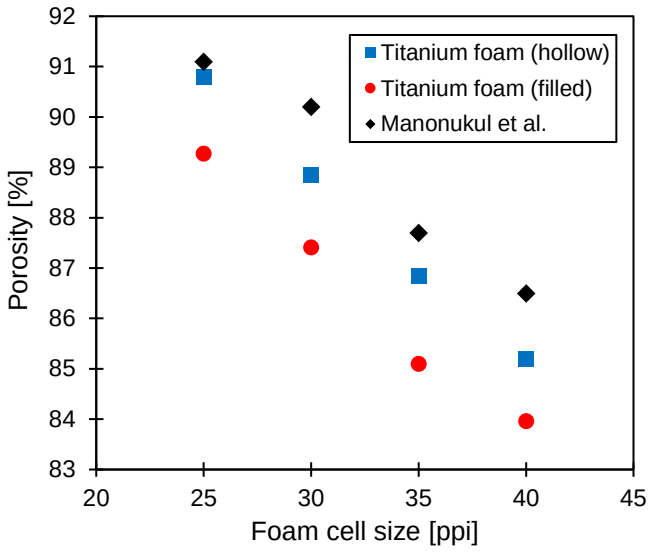

Figure 18 Porosity of titanium foams using varired cell size polyurethane foam

3.2 Pore analysis and geometry anisotropy

The size of individual pore and degree of geometry anisotropy in titanium foams could be quantified by the results from X-ray microtomography. First, the 3D volumes of filled titanium foam structure were used to differentiate pore and titanium strut (as shown in Figure 19A). Subsequently, watershed segmentation algorithm was applied to convert the connected open-cell pores into individual closed pores (Figure 19B). Note that any segmented pore located on the boundaries of specimen surface was excluded to ensure a complete pore geometry.

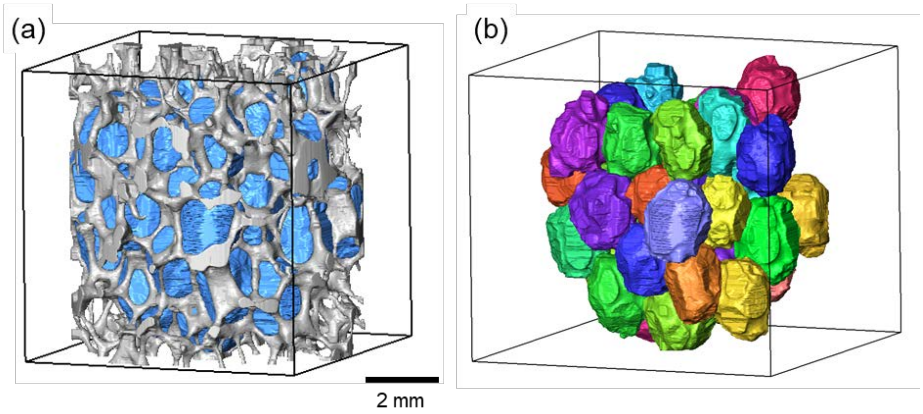

Figure 19 (a) titanium strut and open-cell pores (b) individual closed pores

3.2.1 Pore size and number of pores

Figure 20 demonstrates titanium foam structure and individual closed pores with varied cell size. It can be visualised that there are significant greater number of pores at higher ppi. This is expected since higher ppi meaning that there should be higher number of pores per inch. There are only 24 pores in titanium foam with 25 ppi polyurethane template but this increases to 227 pores in titanium foam with 40 ppi template. In addition, it can be clearly seen that the size of each individual pores decreases with increasing ppi.

Quantification of individual pore size and number of pores with varied cell size was performed and the result is shown in Figure 21. Pore size was measured by calculating equivalent diameter from 3D volume of each pore (assuming spherical pore shape).

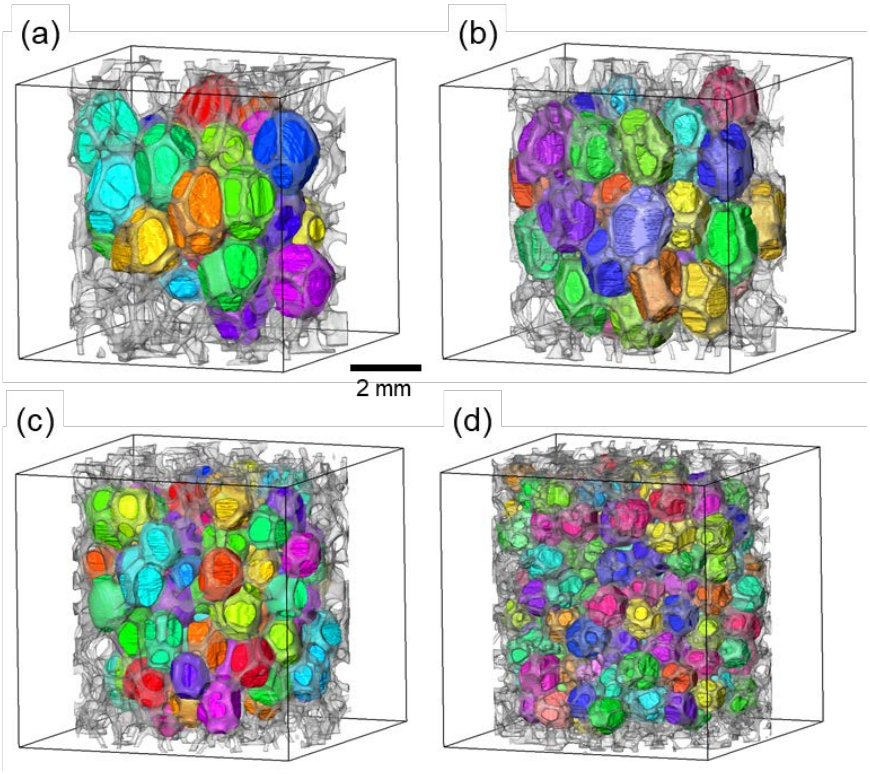

Figure 20 Titanium foam structure and individual closed pores with varied cell size: (a) 25ppi (b) 30 ppi (c) 35ppi (d) 40ppi

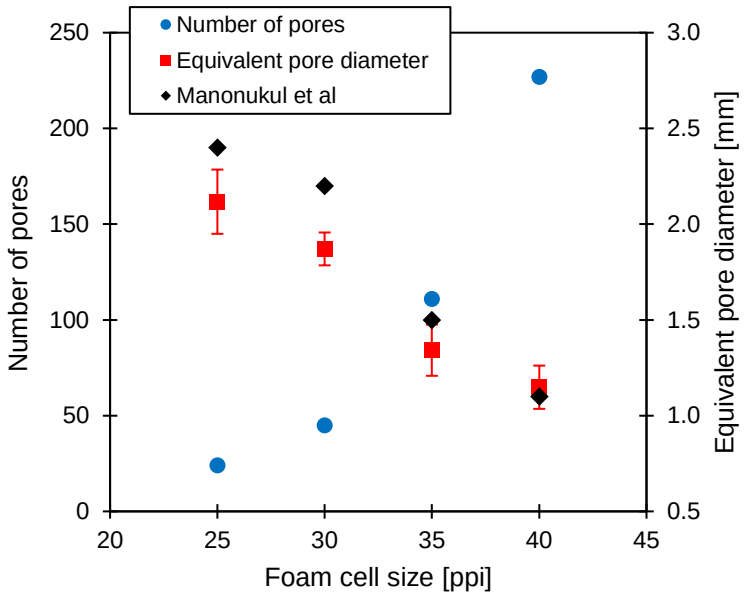

Figure 21 Number of pores and equivalent pore diameter with varired cell size

The results in Figure 21 indicate that the relationship between number of pores and cell size (ppi) is non-linear. The increase in number of pores is more pronounce at higher ppi. It is worth nothing that the measured number of pores here only include those with complete shape. Pores that are located on the boundaries of specimen surface were excluded. This pore exclusion might have a slightly greater effect on the total number of pores, however the authors believe this non-linear relationship is still valid since the 3D analysed volume used in this study is sufficiently large and the analysed number of pores are over 100 in 35 ppi and 40ppi foams.

The average pore diameter decreases with increasing ppi, which is opposite to the number of pores as aforementioned. As shown in Figure 21, average pore diameter is 2.12 mm in 25 ppi foam and 1.87 mm in 30 ppi foam but decreases to 1.34 mm and 1.15 mm in 35 ppi and 40 ppi foams respectively. This is slightly smaller than the average pore size reported by Manonukul et al. [44] since their measurement of pore size using three-dimensional optical microscope (3D-OM) included one strut thickness.

In this research, 2D microstructures were also taken and investigated using 3D optical microscope to confirm with the 3D measurement. The measured average pore diameter (exclude strut thickness) was 1.86 mm in 30 ppi foam, as shown in Figure 22. This is in good agreement with the 3D results.

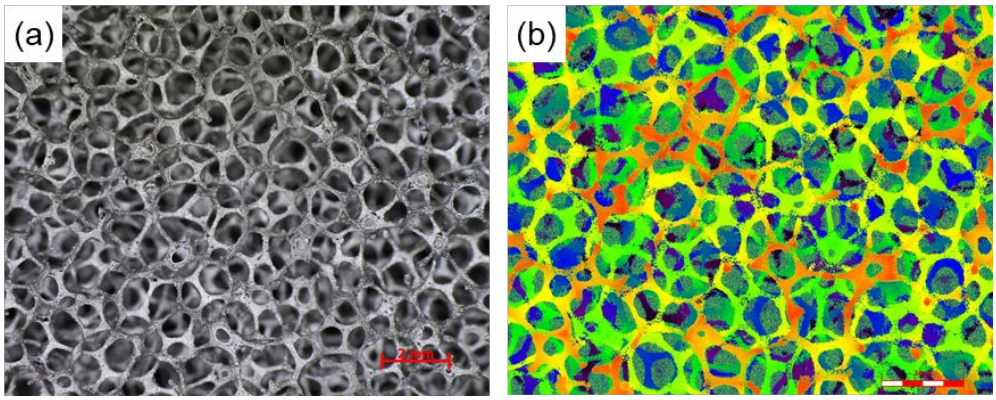

Figure 22 (a) optical micrograph and (b) 3D optical micrograph of 30 ppi titanium foam

3.2.2 Geometry anisotropy

To investigate geometry anisotropy of titanium foam, principal component analysis was performed on each 3D individual pore to determine the aspect ratio (i.e. length along major axis to length along minor axis) and orientation (i.e. angle that the major axis inclided to the foaming direction), as plotted in Figure 23. The average aspect ratio was found to be in a range between 1.33 to 1.39. Note that the aspect ratio becomes unity if a pore is circular, while aspect ratio departs from 1 if a pore become more elongated (higher degree of geometry anisotropy). This indicates the geometry anisotropy of pore and titanium foam manufactured from impregnation method. This explains by the fact that polyurethane foam template was made by foaming method thus having elongated pore in the foaming direction. Similar geometry anisotropy in polyurethane foam was reported elsewhere [45].

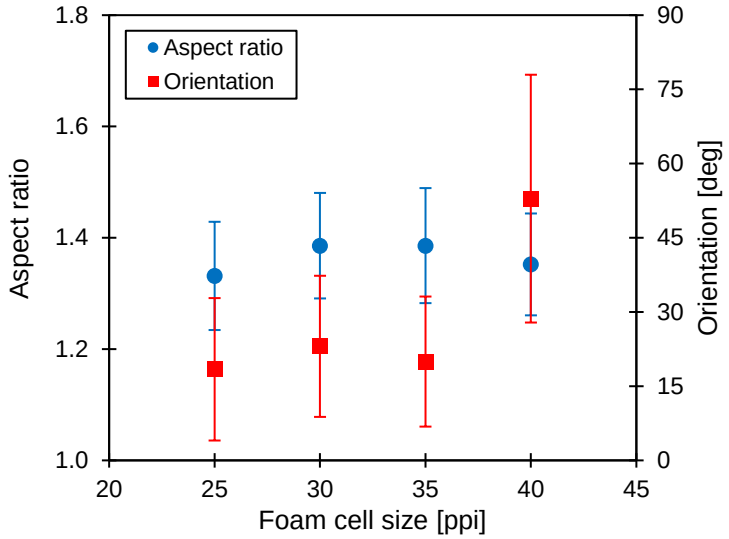

Figure 23 Average aspect ratio and orientation with varired cell size

Orientation of each 3D individual pore can also be used to indicate the degree of geometry anisotropy. The average orientation (angle of major axis inclined to foaming direction) was around 20.5° for the 25 ppi, 30 ppi and 35 ppi titanium foams and was 50.9° for 40 ppi foam. The angle towards 0° and 90° indicates high degree of geometry anisotropy while angle around 45° indicates low degree of geometry anisotropy. The results in Figure 23 confirm

that geometry anisotropy of titanium foam manufactured from impregnation method exist. Titanium foam with 40 ppi polyurethane template appears to have less degree of geometry anisotropy. Previous research [45] also reported that anisotropy decreases with a higher apparent density. Note that measured orientation of pore was found to be relatively random as seen in large value of standard deviation in Figure 23.

To confirm the result from 3D measurement, investigation of pore geometry was further carried out using 3D optical microscopy (3D-OM) and scanning electron microscopy (SEM) as shown in Figure 24 to Figure 25. Micrographs were taken from top view and side view of the samples.

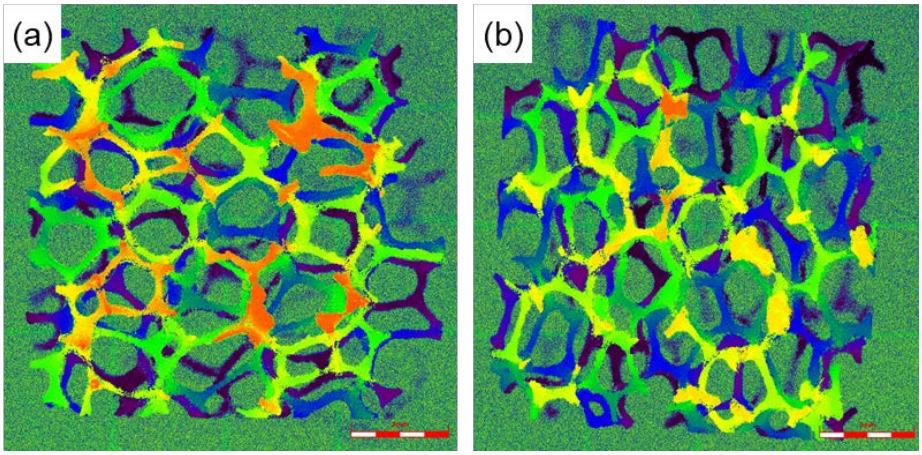

Figure 24 3D optical micrograph of 30 ppi titanium foam (a) top view and (b) side view

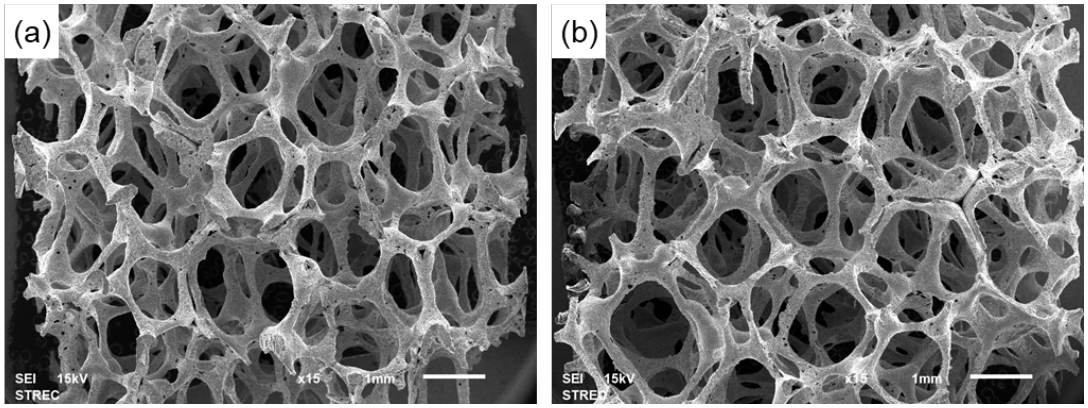

Figure 25 SEM micrograph of 30 ppi titanium foam (a) top view and (b) side view

It can be clearly observed that pore geometry is more elongated in the side view as compared to the top view (both in 3D-OM and SEM micrographs) since the foaming direction is along vertical direction of the specimen. From 3D-OM result, length measurement along major and minor axes was also performed using image analysis software to estimate the aspect ratio. It was found that the average aspect ratio of 30 ppi titanium foam was 1.31, which agrees well with 3D measurement in the previous section. It is confirmed that titanium foams made from replica impregnation method could have certain degree of geometry anisotropy.

3.3 Pore distribution and strut network

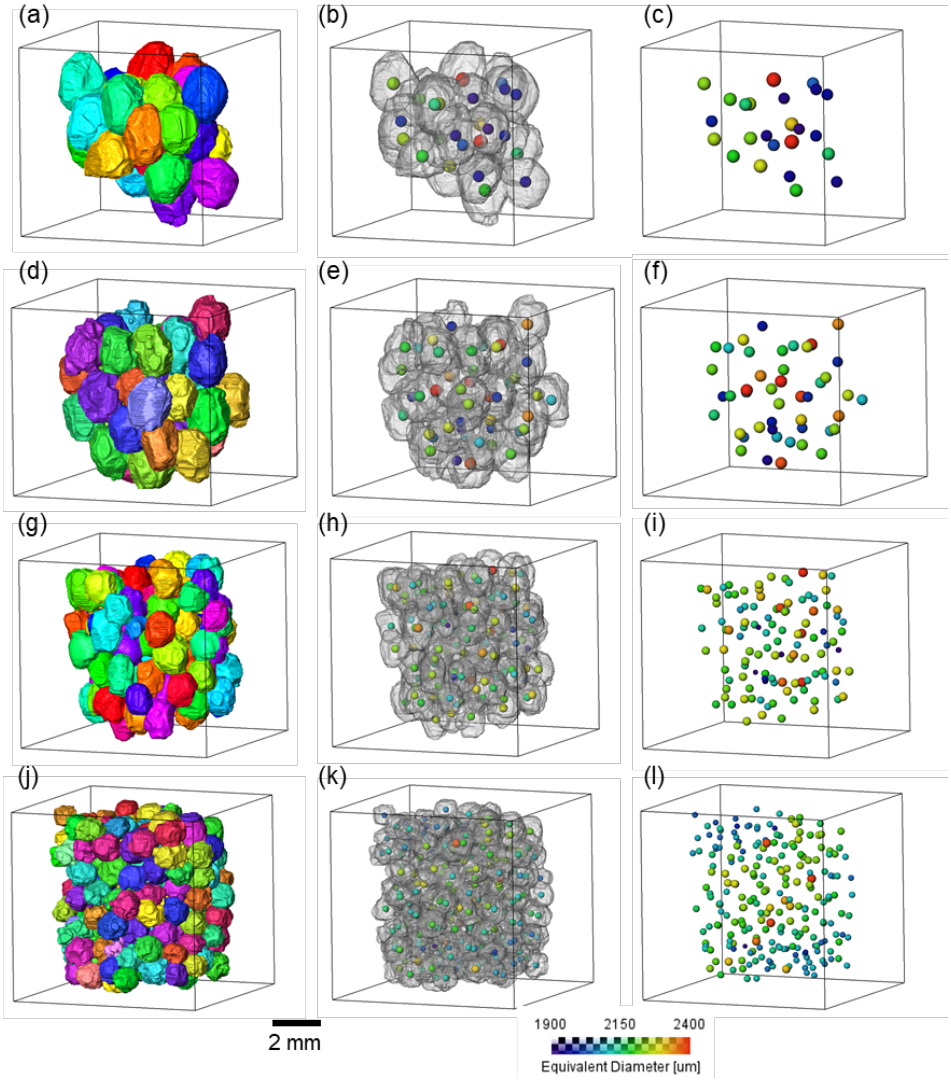

Figure 26 Location and size of individual pore (a-c) 25 ppi, (d-f) 30 ppi, (g-i) 35 ppi, (j-l) 40 ppi

Location and size of each individual pore was investigated and shown in Figure 26. Location of each pore was identified by its centroid and equivalent pore diameter was used to label each pore with different colour based on its pore size. It can be clearly seen that pores are distributed uniformly throughout the specimen. No area of pore cluster was observed. Pore size was also evenly distributed. Distribution of pore size was also quantified and shown in Figure 27.

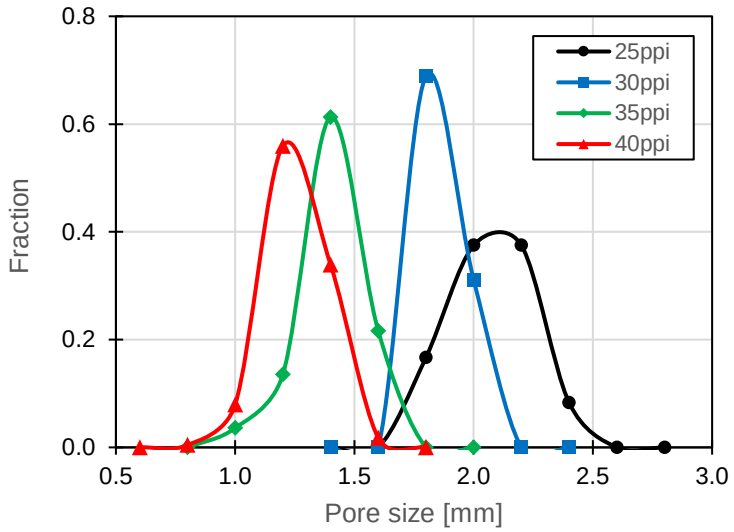

Figure 27 Pore size distribution with varired cell size

Normal (symmetry) distribution of pore size was observed in all four samples. Titanium foam with 25 ppi template appears to have broadest size distribution whereas 30 ppi titanium foam appears to have narrowest size distribution. The width of size distribution in all foams is approximately 0.5 mm. This is in contrast with prior work [43] reported that the distribution of pore size was non-symmetric and slightly skewed to smaller sizes. The efficacy of 3D analysis proves to be beneficial to in-depth analysis of individual pore.

Quantification of interconnected network of titanium strut was also performed using skeletonization method. First, distance map of the segmented titanium strut was calculated. Subsequently, thinning process was performed based on the distance map to

obtain a string of connected voxels. Finally, the connected voxels were converted to a spatial graph consisting of nodes and vertices. Nodes and vertices represent interconnect and strut in titanium foam structure, respectively. The strut networks, consisting of nodes and vertices, of all four titanium foams are presented in Figure 28.

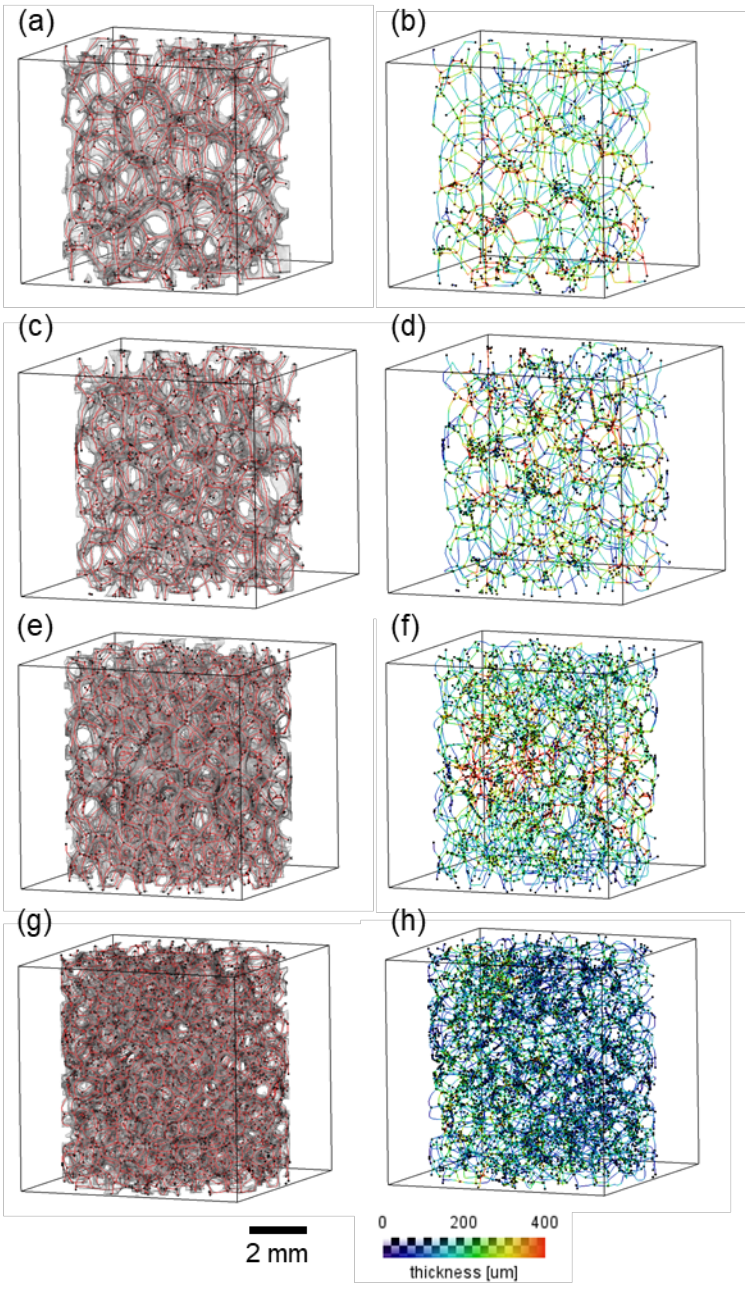

Figure 28 Strut network and strut thickness of (a) 25 ppi, (b) 30 ppi, (c) 35 ppi, (d) 40 ppi

The thickness of each strut (i.e. vertices) can also be quantified to identify the uniformity of titanium strut thickness from replica impregnation method, as shown in Figure 28. It can be observed that distribution of strut thickness is relatively uniform in all samples, except the titanium foam with 35 ppi template that show an area of slightly thicker struts in the middle part of the sample. This might be because of 2 possible scenarios: (1) air bubbles were introduced during titanium slurry coating process and (2) cleaning (after coating) cannot fully reach the middle part of the sample. Since the analysis was done on the filled titanium structure, any internal/surface-connected void would be filled and considered as strut for network analysis, thus making struts with surface-connected voids become thicker. The authors believe that the first scenario is more likely as it agrees well with the aforementioned result shown in Figure 13c that titanium foam with 35 ppi template has the most air bubbles (most of them are located near the middle part of the sample). The insights from this analysis could be further utilized to achieve optimized process parameters for manufacturing of titanium foam with uniform strut thickness.

Figure 29 illustrates average strut thickness of titanium foams with varired cell size. Variation in thickness is rather high and there is no clear relationship between strut thickness and template cell size.

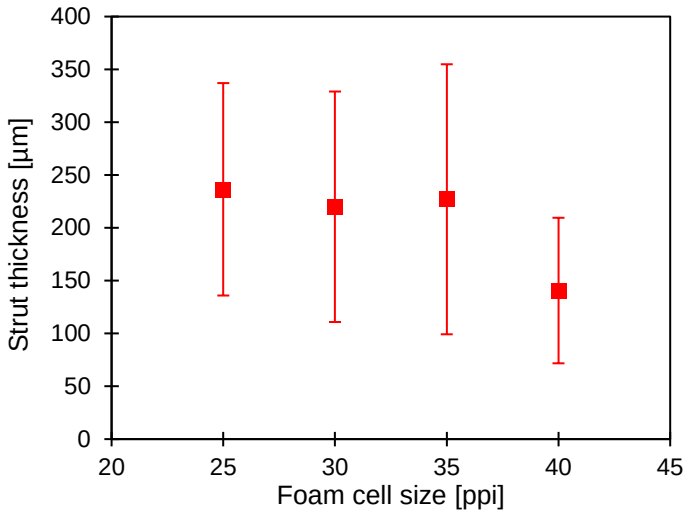

Figure 29 Average strut thickness with varired cell size

3.4 Fluid flow simulation

Tomographic-based CFD simulation of flow through open-cell structures was performed on all four specimens with the same size (4x4x4 mm^3) of representative elementary volume (REV), as shown in Figure 6. The flow studies were carried out in each of the three directions along the x, y and z axes. The x and y axes represent the direction perpendicular to foaming direction while z axis represents the direction parallel to foaming direction.

The pressure contourand flow velocities from the flow simulations are shown in Figure 30 and Firgure 31, respectively. Planar cross-section for 2D visualization can be done either in parallel plane or perpendicular plane to the flow direction.

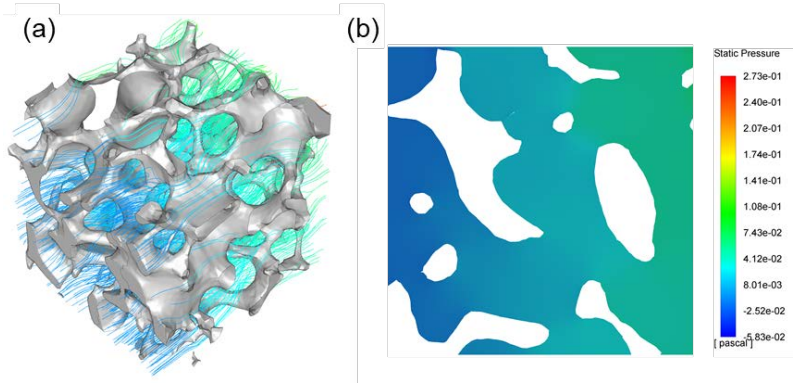

Figure 30 Visualization of the pressure contour inside 30 ppi foam: (a) 3D flow and (b) 2D cross-section

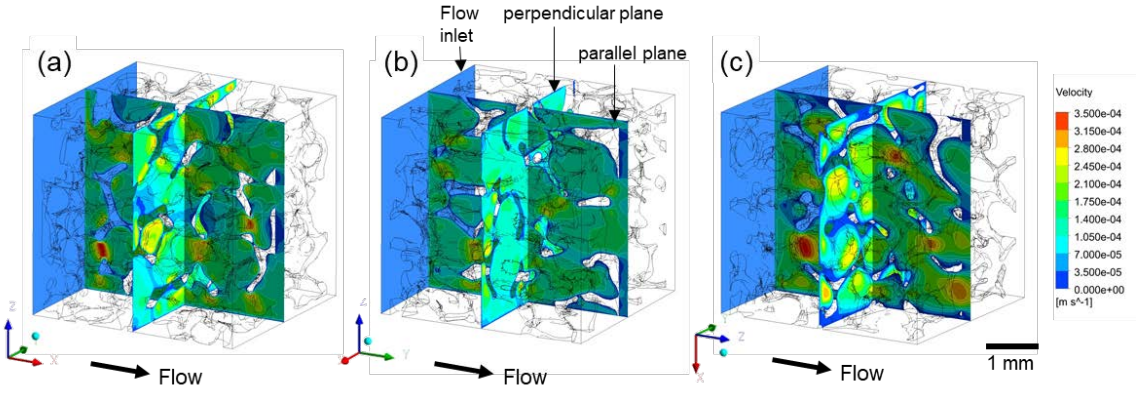

Figure 31 Visualization of the velocity contour inside 30 ppi foam: (a-b) flow perpendicular to foaming direction and (c) flow along foaming direction. Note that two cross-sectional planes are shown to represent the plane parallel and perpendicular to the flow direction

3.4.1 Flow velocity through open-cell titanium foams

Flow velocity magnitudes resulting from the flow simulations in the x direction, perpendicular to foaming direction, are shown in Figure 32 and Figure 33.

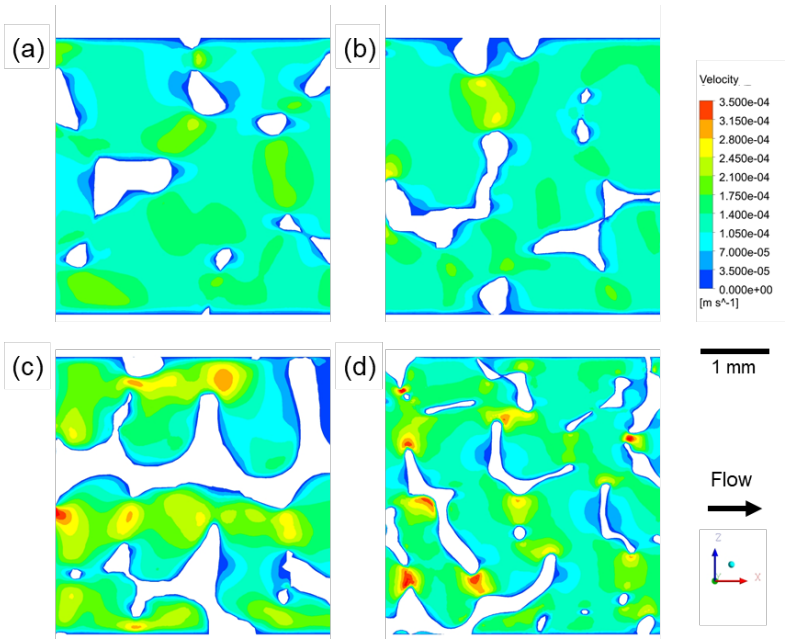

Figure 32 2D cross-sectional views (parallel plane) of the 3D velocity magnitudes along x-direction showing fluid flow within titanium foams (a) 25 ppi (b) 30 ppi (c) 35 ppi (d) 40 ppi

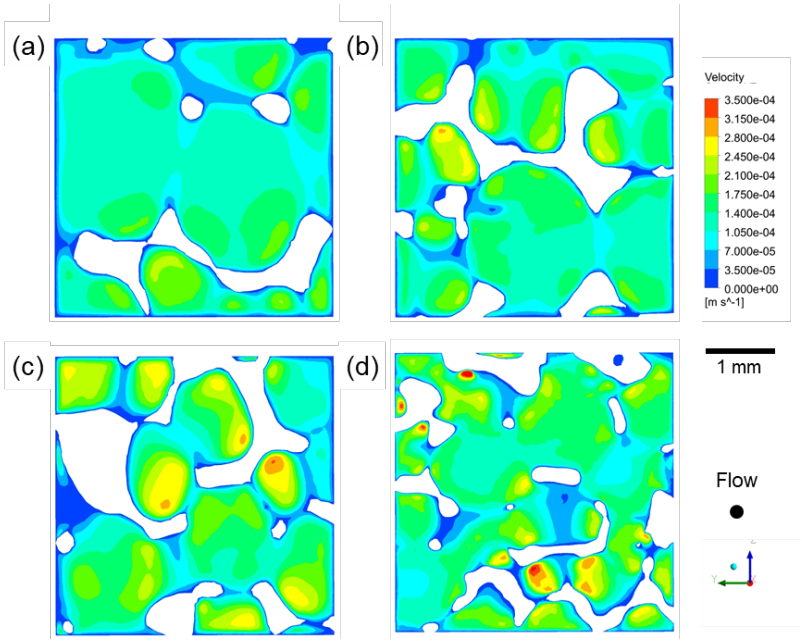

Figure 33 2D cross-sectional views (perpendicular plane) of the 3D velocity magnitudes along x-direction showing fluid flow within titanium foams (a) 25 ppi (b) 30 ppi (c) 35 ppi (d) 40 ppi

Flow velocity magnitudes resulting from the flow simulations in the z direction, parallel to foaming direction, are shown in Figure 34 and Figure 35.

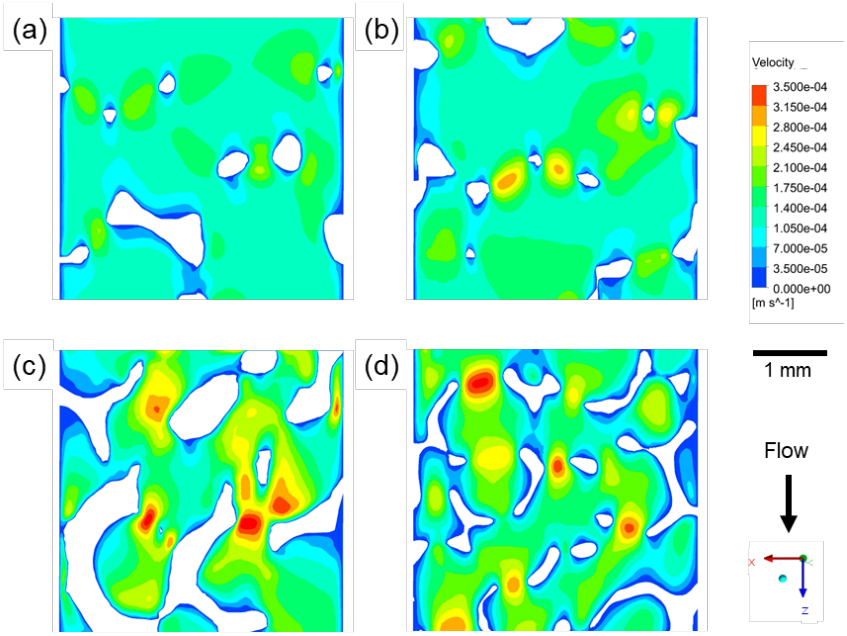

Figure 34 2D cross-sectional views (parallel plane) of the 3D velocity magnitudes along z-direction showing fluid flow within titanium foams (a) 25 ppi (b) 30 ppi (c) 35 ppi (d) 40 ppi

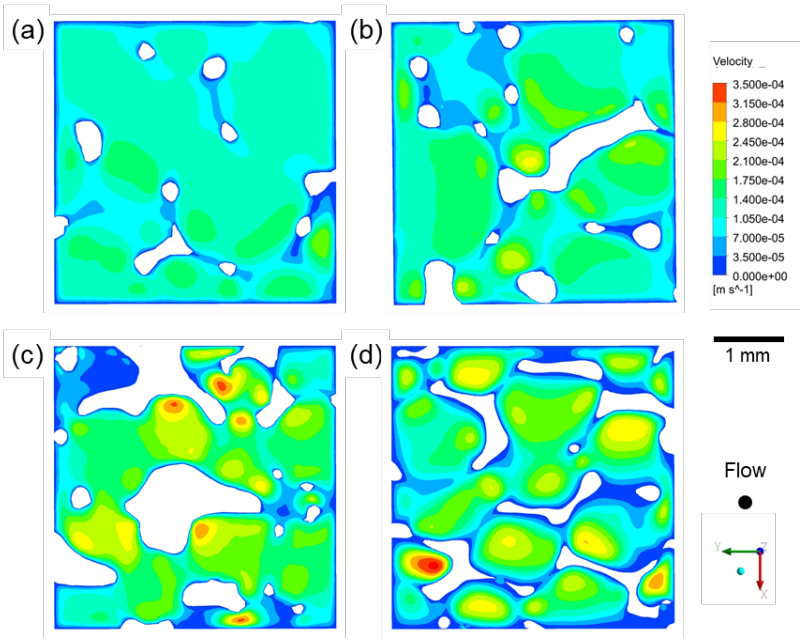

Figure 35 2D cross-sectional views (perpendicular plane) of the 3D velocity magnitudes along z-direction showing fluid flow within titanium foams (a) 25 ppi (b) 30 ppi (c) 35 ppi (d) 40 ppi

From a qualitative perspective, the results shown in Figures 32 – 35 demonstrate that pore interconnects strongly block the fluid flow, particularly at higher ppi foam (lower pososity). This is expected as pore interconnects have smaller channel size for the fluid flow as compared to the open pore space and these channels become even smaller at higher ppi (lower porosity). Considering the direction of flow, flows perpendicular to foaming direction (x-direction) seem to be slightly rougher since the interconnects are rather complex and random (Figures 32-33). In contrast, flows parallel to foaming direction (z-direction) seem to have less blockage since the interconnects are less complex (Figures 34-35). The different in fluid-flow emphasizes that geometry anisotropy of titanium foams could result in different flow behaviour.

3.4.2 Permeability assessment of titanium foams

The permeabilities of titanium foams with varied cell size were calculated based on Darcy's Law, as described in method section, and shown in Figure 36.

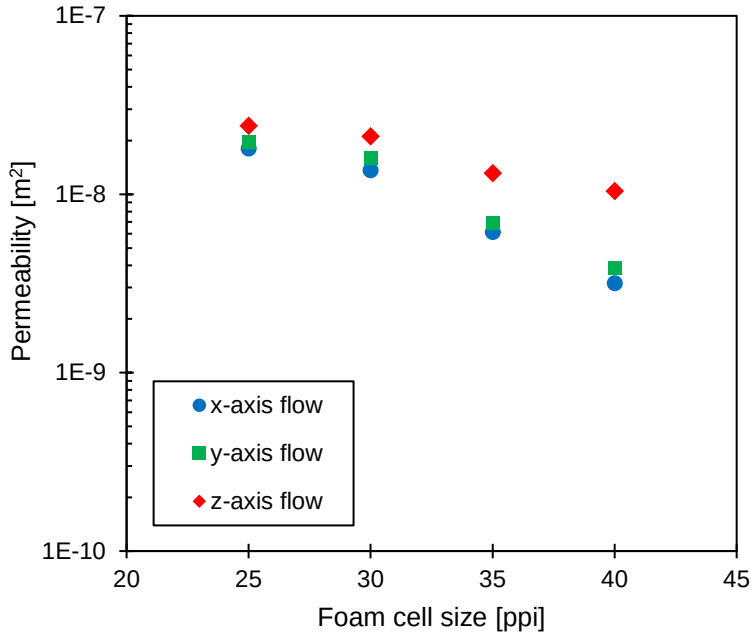

Figure 36 Permeability for fluid flow in titanium foams with varired cell size

The permeability is significantly higher for the flow parallel to foaming direction (z-direction) as compared to the flow perpendicular to foaming direction (x- and y- directions). Note that the different in permeability is more pronounce towards higher ppi foams. The variation in permeability with foaming direction confirms that the degree of geometry anisotropy was sufficient to cause significant flow property anisotropy. Previous strudy also indicated that sufficient geometry anisotropy is needed to create mechanical property anisotropy [44].

Figure 37 illustrates permeability of foam structures with level of porosity. The permeabiliy increases with higher porosity. The result from preliminary liquid-flow experiment in this study was also added in Figure 37. The measured permeability was in the same order of magnitude but was slightly lower than that from numerical simulation. To confirm the accuracy of numerical simulation in this work, permeabilities from various literatures (from both numerical and experimental studies) [18, 39, 41, 46] were also included in Figure 37. A good agreement between the results in this work and the previous studies can be observed.

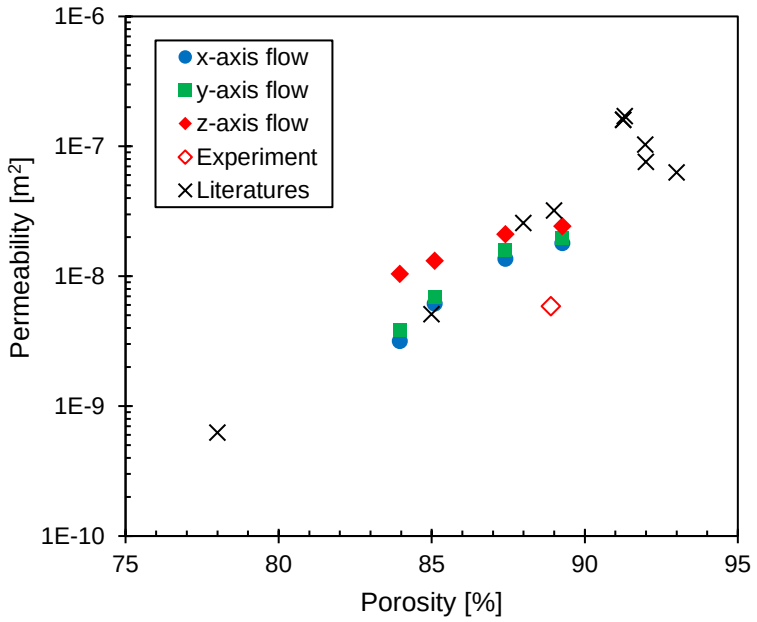

Figure 37 Permeability for fluid flow in titanium foams with varired cell size

Conclusion

Open-cell titanium foams have been receiving growing attention from the industrial to be used in biological and functional engineering applications due to their lightweight porous structure with excellent physical and mechanical properties. Prior studies suggested that structural difference in manufactured titanium foams can greatly affect flow behaviour. Therefore, there is a strong need to accurately quantify structural geometry and morphology of porous networks and their effects on flow properties. In this proposed project, the x-ray tomography technique was used to characterise actual structure of open-cell titanium foams, manufactured from replica impregnation method. Titanium foams with four different porosity, produced using polymer template with porosity of 25-40 ppi (pore per linear inch), were studied. It was found that titanium foam manufactured from replica impregnation method has the characteristic hollow strut, containing polyurethane voids and air bubbles. The results also indicated that that polyurethane template was not well covered by titanium powder in some areas, particularly near the interconnect of struts. In addition, air bubbles were found throughout the specimens near the surface of titanium strut. This is likely that air entrapement occurs during titanium slurry coating process.

In-depth analysis was performed to quantify structural parameters and morphological geometries of open-cell pores and titanium struts. As the template cell size (ppi) increased, porosity and average pore diameter decreased whereas the number of individual pores increased. The average aspect ratio was found to be in a range between 1.33 to 1.39. The average orientation (angle of major axis inclined to foaming direction) was around 20.5°. The measured aspect ratio and orientation of pores indicated geometry anisotropy of titanium foams. Microstructure evaluation using scanning electron microscope and 3D optical microscope confirmed geometry anisotropy of the structure. The average strut thickness of titanium foams was around 220 um.

The numerical analysis and permeability assessment of fluid flow were also performed to investigate the relationship between structural parameters and flow behaviour. The permeability was significantly higher for the flow parallel to foaming direction as compared to the flow perpendicular to foaming direction, confirming that degree of geometry anisotropy was sufficient to cause significant flow property anisotropy. This better insight is of great importance to design the optimal structure for various functional applications.

References

1. Boyer, R.R., *An overview on the use of titanium in the aerospace industry.* Materials Science and Engineering: A, 1996. **213**(1–2): p. 103-114.
2. Peters, M., et al., *Structure and Properties of Titanium and Titanium Alloys*, in *Titanium and Titanium Alloys*. 2005, Wiley-VCH Verlag GmbH & Co. KGaA. p. 1-36.
3. Ashby, M.F., et al., *Metal Foams: A Design Guide*. 2000, Burlington, MA: Butterworth-Heinemann, Elsevier Science.
4. Banhart, J., *Manufacture, characterisation and application of cellular metals and metal foams.* Progress in Materials Science, 2001. **46**(6): p. 559-632.
5. Asavavisithchai, S. and A.R. Kennedy, *The effect of Mg addition on the stability of Al–Al2O3 foams made by a powder metallurgy route.* Scripta Materialia, 2006. **54**(7): p. 1331-1334.
6. Manonukul, A., et al., *Effects of replacing metal powder with powder space holder on metal foam produced by metal injection moulding.* Journal of Materials Processing Technology, 2010. **210**(3): p. 529-535.
7. Salvo, L., et al., *Processing and structures of solids foams.* Comptes Rendus Physique, 2014. **15**(8–9): p. 662-673.
8. Dunand, D.C., *Processing of Titanium Foams.* Advanced Engineering Materials, 2004. **6**(6): p. 369-376.
9. Singh, R., et al., *Titanium foams for biomedical applications: a review.* Materials Technology, 2010. **25**(3-4): p. 127-136.
10. Kim, T.B., et al., *Additive manufactured porous titanium structures: Through-process quantification of pore and strut networks.* Journal of Materials Processing Technology, 2014. **214**(11): p. 2706-2715.
11. Rak, Z.S. and J. Walter, *Porous titanium foil by tape casting technique.* Journal of Materials Processing Technology, 2006. **175**(1–3): p. 358-363.
12. Chen, Y.J., et al., *Fabrication of porous titanium implants with biomechanical compatibility.* Materials Letters, 2009. **63**(30): p. 2659-2661.

13. Niu, W., et al., *Processing and properties of porous titanium using space holder technique.* Materials Science and Engineering: A, 2009. **506**(1–2): p. 148-151.
14. Esen, Z. and Ş. Bor, *Characterization of Ti–6Al–4V alloy foams synthesized by space holder technique.* Materials Science and Engineering: A, 2011. **528**(7–8): p. 3200-3209.
15. Tuncer, N., et al., *Investigation of spacer size effect on architecture and mechanical properties of porous titanium.* Materials Science and Engineering: A, 2011. **530**(0): p. 633-642.
16. Zhao, J., X. Lu, and J. Weng, *Macroporous Ti-based composite scaffold prepared by polymer impregnating method with calcium phosphate coatings.* Materials Letters, 2008. **62**(17–18): p. 2921-2924.
17. Manonukul, A., et al., *Rheological properties of commercially pure titanium slurry for metallic foam production using replica impregnation method.* Powder Technology, 2014. **266**(0): p. 129-134.
18. Singh, R., et al., *Characterization of the structure and permeability of titanium foams for spinal fusion devices.* Acta biomaterialia, 2009. **5**(1): p. 477-487.
19. Zhang, Z., et al., *Hierarchical tailoring of strut architecture to control permeability of additive manufactured titanium implants.* Materials Science and Engineering: C, 2013. **33**(7): p. 4055-4062.
20. Dai, Z., et al., *A Comparison of Metal-Foam Heat Exchangers to Compact Multilouver Designs for Air-Side Heat Transfer Applications.* Heat Transfer Engineering, 2011. **33**(1): p. 21-30.
21. Zhao, C.Y., *Review on thermal transport in high porosity cellular metal foams with open cells.* International Journal of Heat and Mass Transfer, 2012. **55**(13–14): p. 3618-3632.
22. Grigoriev, S.A., et al., *Optimization of porous current collectors for PEM water electrolysers.* International Journal of Hydrogen Energy, 2009. **34**(11): p. 4968-4973.
23. Huisseune, H., et al., *Simulation of an Aluminum Foam Heat Exchanger Using the Volume Averaging Technique.* Procedia Materials Science, 2014. **4**(0): p. 334-339.

24. Minko, K.B., V.I. Artemov, and G.G. Yan'kov, *Numerical study of hydrogen purification using metal hydride reactor with aluminium foam.* Applied Thermal Engineering, 2015. **76**(0): p. 175-184.

25. Mancin, S., et al., *Air forced convection through metal foams: Experimental results and modeling.* International Journal of Heat and Mass Transfer, 2013. **62**(0): p. 112-123.

26. Zafari, M., et al., *Microtomography-based numerical simulation of fluid flow and heat transfer in open cell metal foams.* Applied Thermal Engineering, 2015. **80**(0): p. 347-354.

27. Boomsma, K. and D. Poulikakos, *The Effects of Compression and Pore Size Variations on the Liquid Flow Characteristics in Metal Foams.* Journal of Fluids Engineering, 2001. **124**(1): p. 263-272.

28. Khayargoli, P., et al. *The Impact of Microstructure on the Permeability of Metal Foams*. in *CSME Forum*. 2004. Ontario, Canada.

29. Ranut, P., E. Nobile, and L. Mancini, *High resolution X-ray microtomography-based CFD simulation for the characterization of flow permeability and effective thermal conductivity of aluminum metal foams.* Experimental Thermal and Fluid Science, 2015. **67**(0): p. 30-36.

30. Despois, J.-F. and A. Mortensen, *Permeability of open-pore microcellular materials.* Acta Materialia, 2005. **53**(5): p. 1381-1388.

31. Puncreobutr, C., et al., *Coupling in situ synchrotron X-ray tomographic microscopy and numerical simulation to quantify the influence of intermetallic formation on permeability in aluminium–silicon–copper alloys.* Acta Materialia, 2014. **64**(0): p. 316-325.

32. Maire, E. and P.J. Withers, *Quantitative X-ray tomography.* International Materials Reviews, 2014. **59**(1): p. 1-43.

33. Puncreobutr, C., et al., *Quantitative 3D characterization of solidification structure and defect evolution in Al alloys.* JOM Journal of the Minerals, Metals and Materials Society, 2012. **64**(1): p. 89-95.

34. Yue, S., et al., *Evaluation of 3-D bioactive glass scaffolds dissolution in a perfusion flow system with x-ray microtomography.* Acta Biomaterialia, 2011. **7**(6): p. 2637-2643
35. Bock, J. and A.M. Jacobi, *Geometric classification of open-cell metal foams using X-ray micro-computed tomography.* Materials Characterization, 2013. **75**(0): p. 35-43.
36. Boomsma, K., D. Poulikakos, and Y. Ventikos, *Simulations of flow through open cell metal foams using an idealized periodic cell structure.* International Journal of Heat and Fluid Flow, 2003. **24**(6): p. 825-834.
37. Krishnan, S., S.V. Garimella, and J.Y. Murthy, *Simulation of Thermal Transport in Open-Cell Metal Foams: Effect of Periodic Unit-Cell Structure.* Journal of Heat Transfer, 2008. **130**(2): p. 024503-024503.
38. Moreno-Atanasio, R., R.A. Williams, and X. Jia, *Combining X-ray microtomography with computer simulation for analysis of granular and porous materials.* Particuology, 2010. **8**(2): p. 81-99.
39. Bodla, K.K., J.Y. Murthy, and S.V. Garimella, *Microtomography-Based Simulation of Transport through Open-Cell Metal Foams.* Numerical Heat Transfer, Part A: Applications, 2010. **58**(7): p. 527-544.
40. Diani, A., et al., *Numerical Analysis of Air Flow through Metal Foams.* Energy Procedia, 2014. **45**(0): p. 645-652.
41. Ranut, P., E. Nobile, and L. Mancini, *Microtomography-based CFD Analysis of Transport in Open-Cell Aluminum Metal Foams.* Journal of Physics: Conference Series, 2014. **501**(1): p. 012021.
42. Puncreobutr, C., et al., *Synchrotron tomographic characterization of damage evolution during aluminum alloy solidification.* Metallurgical and Materials Transactions A, 2013. **44**(12): p. 5389-5395.
43. Manonukul, A., P. Srikudvien, and M. Tange, *Microstructure and mechanical properties of commercially pure titanium foam with varied cell size fabricated by replica impregnation method.* Materials Science and Engineering: A, 2016. **650**: p. 432-437.

44. Manonukul, A., et al., *Geometry anisotropy and mechanical property isotropy in titanium foam fabricated by replica impregnation method.* Materials Science and Engineering: A, 2016. **655**: p. 388-395.
45. Ridha, M. and V.P.W. Shim, *Microstructure and Tensile Mechanical Properties of Anisotropic Rigid Polyurethane Foam.* Experimental Mechanics, 2008. **48**(6): p. 763.
46. Innocentini, M.D.M., et al., *Prediction of ceramic foams permeability using Ergun's equation.* Materials Research, 1999. **2**: p. 283-289.